

การแลกเปลี่ยนของสปีชีส์คอปเปอร์ไนโตรเจนแซดเอเอ็ม-5 ที่ปริมาณคอปเปอร์ต่ำ



นางสาวเพ็ญกัญญา อุ๋นจิตต์

สถาบันวิทยบริการ
จุฬาลงกรณ์มหาวิทยาลัย
วิทยานิพนธ์นี้เป็นส่วนหนึ่งของการศึกษาตามหลักสูตรปริญญาวิทยาศาสตรมหาบัณฑิต

สาขาวิชาเคมี ภาควิชาเคมี

คณะวิทยาศาสตร์ จุฬาลงกรณ์มหาวิทยาลัย

ปีการศึกษา 2547

ISBN 974-17-6080-9

ลิขสิทธิ์ของจุฬาลงกรณ์มหาวิทยาลัย

**EXCHANGE OF COPPER SPECIES IN THE CAVITY OF ZSM-5
AT LOW COPPER LOADING**



Miss Pengunya Unjit

**สถาบันวิทยบริการ
จุฬาลงกรณ์มหาวิทยาลัย**
**A Thesis Submitted in Partial Fulfillment of the Requirements
for the Degree of Master of Science in Chemistry**

Department of Chemistry

Faculty of Science

Chulalongkorn University

Academic Year 2004

ISBN 974-17-6080-9

Thesis Title EXCHANGE OF COPPER SPECIES IN THE CAVITY OF ZSM-5
AT LOW COPPER LOADING
By Miss Pengunya Unjit
Field of Study Chemistry
Thesis Advisor Associate Professor Vudhichai Parasuk, Ph.D.

Accepted by Faculty of Science, Chulalongkorn University in Partial
Fulfillment of the Requirements for the Master's Degree

.....Dean of the Faculty of Science
(Professor Piamsak Menasveta, Ph.D.)

THESIS COMMITTEE

.....Chairman
(Associate Professor Sirirat Kokpol, Ph.D.)

.....Thesis Advisor
(Associate Professor Vudhichai Parasuk, Ph.D.)

.....Member
(Associate Professor Supot Hannongbua, Ph.D.)

.....Member
(Aticha Chaisuwan, Ph.D.)

เพ็ญกันยา อุ่นจิตต์ : การแลกเปลี่ยนของสปีชีส์คอปเปอร์ในโพรงแซดเอเอ็ม-5 ที่ปริมาณคอปเปอร์ต่ำ (EXCHANGE OF COPPER SPECIES IN THE CAVITY OF ZSM-5 AT LOW COPPER LOADING) อาจารย์ที่ปรึกษา: รศ. ดร. วุฒิชัย พาราสุข, 92 หน้า, ISBN 974-17-6080-9

ได้มีการคำนวณด้วยทฤษฎีเด้นซิติฟังก์ชันนัล เพื่อศึกษาการแลกเปลี่ยน Cu^{2+} และ Cu^+ และการเกิดออกโตรีดักชันของ Cu^{2+} ไปเป็น Cu^+ ในโพรง ZSM-5 ที่บริเวณตำแหน่งแลกเปลี่ยน T6T12, T8T8, T7T12-model1 และ T7T12-model2 การหาโครงสร้างเสถียรทั้งหมดในการศึกษานี้หาด้วยวิธี B3LYP/6-31G(d,p) เพื่อให้ได้มาซึ่งโครงสร้างของ ZSM-5 ได้มีการทำการคำนวณด้วยวิธีโมเลกุลาร์ไดนามิกซิมูเลชันบนโครงสร้าง MFI ที่มีการแทนที่ Si 2 อะตอมด้วย Al 2 อะตอม และจุดประจุลบที่เกิดขึ้นมาด้วย H^+ 2 อนุภาค แบบจำลองคลัสเตอร์ชนิดวง 5- และ 6-T สร้างจากโครงสร้าง HZSM-5 ที่ได้จากการคำนวณ โดยที่อะตอม O ที่ตำแหน่งปลายแบบจำลองคลัสเตอร์ ให้เชื่อมตัวด้วยอะตอม H พารามิเตอร์ทางโครงสร้างทั้งหมดของแบบจำลองคลัสเตอร์จะถูกรักษาให้คงที่ ยกเว้นตำแหน่ง H^+ พันธะ O-H และ มุมพันธะ T-O-H (\angle T-O-H) ผลจากการหาโครงสร้างเสถียรได้ค่า O-H เป็น 0.96 Å และ \angle T-O-H อยู่ระหว่าง 115.33° - 118.98° สำหรับแบบจำลองคลัสเตอร์ของ CuZSM-5 สร้างจากแบบจำลองคลัสเตอร์ของ HZSM-5 โดยแทนที่ H^+ ด้วย 1 Cu^{2+} หรือ 1 Cu^+ สำหรับ CuZSM-5 ที่มีการแลกเปลี่ยนด้วยไอออน 1 ไอออน หรือ 2 Cu^+ สำหรับ CuZSM-5 ที่มีการแลกเปลี่ยนด้วยไอออน 2 ไอออน มีการหาตำแหน่งที่เสถียรเฉพาะตำแหน่ง H^+ , Cu^+ และ Cu^{2+} พบว่าระยะ O-H⁺, Cu^{2+} -O และ Cu^+ -O มีระยะอยู่ระหว่าง 0.97-1.00 Å, 1.92-4.17 Å และ 1.75-5.33 Å ตามลำดับ สำหรับบริเวณการแลกเปลี่ยนทั้งหมด พบว่าสปีชีส์ Cu เกิดทั้ง mono- และ bi-coordination กับ ZSM-5 เมื่อพิจารณาถึงพลังงานการแลกเปลี่ยน (ΔE_{exch}) บริเวณการแลกเปลี่ยนทั้งหมดมีพลังงานเป็นบวก สปีชีส์ Cu แลกเปลี่ยนที่เสถียรที่สุดคือ Cu^{2+} และบริเวณการแลกเปลี่ยนที่ดีที่สุดคือ T6T12 โดยมีค่า ΔE_{exch} เท่ากับ 9.19 กิโลแคลอรีต่อโมล สำหรับการเกิดออกโตรีดักชันของ Cu^{2+} ไปเป็น Cu^+ พลังงานการเกิดออกโตรีดักชัน (ΔE_{auto}) ที่ต่ำสุด คือ 148.93 กิโลแคลอรีต่อโมล โดยเกิดที่บริเวณการแลกเปลี่ยน T7T12-model1 แม้ว่า ΔE_{auto} ของ Cu^{2+} ในโพรง ZSM-5 ต่ำกว่าในสถานะสารละลาย แต่ก็ยังมีค่าสูงมาก จากค่า ΔE_{exch} และ ΔE_{auto} ที่ได้ การแลกเปลี่ยนไอออน Cu และการเกิดออกโตรีดักชันของ Cu^{2+} ไม่น่าจะเกิดขึ้นได้ที่อุณหภูมิห้อง

ภาควิชา.....เคมี..... ลายมือชื่อนิสิต.....
 สาขาวิชา.....เคมี..... ลายมือชื่ออาจารย์ที่ปรึกษา.....
 ปีการศึกษา.....2547.....

4472355123: MAJOR CHEMISTRY

KEYWORD: HZSM-5/ CuZSM-5/ Density Functional Theory/ Exchanged Energy/
Autoreduction Energy

PENGUNYA UNJIT: EXCHANGE OF COPPER SPECIES IN THE CAVITY OF
ZSM-5 AT LOW COPPER LOADING. THESIS ADVISOR: ASSOC. PROF.
VUDHICHAIR PARASUK, Ph.D., 92 pp., ISBN 974-17-6080-9.

Density functional theory calculations were performed to examine exchange of Cu^{2+} and Cu^+ and autoreduction of Cu^{2+} to Cu^+ in the cavity of ZSM-5 at T6T12, T8T8, T7T12-model1, and T7T12-model2 exchanged site. All geometry optimizations were carried out using B3LYP/6-31G(d,p). To obtain ZSM-5 structures, Molecular Dynamic (MD) Simulations were performed on the MFI structure, in which 2 Si atoms were replaced by 2 Al atoms. Two excess negative charges were balanced by 2 H^+ . The cluster models of 5- and 6-T-ring were extracted from the simulated HZSM-5 structures where all terminal oxygen atoms were saturated with H atoms. Geometrical parameters of the cluster were fixed except the position of H^+ , O-H bond lengths (O-H), and T-O-H bond angles ($\angle\text{T-O-H}$). The results from optimizations yielded O-H distances of 0.96 Å and $\angle\text{T-O-H}$ angles of 115.33°-118.98°. For the cluster model of CuZSM-5, HZSM-5 structures were taken and H^+ were replaced either by 1 Cu^{2+} , or 1 Cu^+ for one-ion exchanged CuZSM-5 or 2 Cu^+ for two-ion exchanged CuZSM-5. Only positions of H^+ , Cu^+ , and Cu^{2+} were optimized. For O- H^+ , Cu^{2+} -O, and Cu^+ -O, the distances are between 0.97-1.00 Å, 1.92-4.17 Å, and 1.75-5.33 Å, respectively. For all exchanged sites, Cu species form either mono- or bi- coordination with ZSM-5. When considered exchanged energies (ΔE_{exch}), all CuZSM-5 exchanged sites have positive ΔE_{exch} . The most stable exchanged Cu species is Cu^{2+} and the most favorable exchanged site is T6T12 with ΔE_{exch} of 9.19 kcal/mol. For the autoreduction of Cu^{2+} to Cu^+ , lowest autoreduction energy (ΔE_{auto}) of 148.93 kcal/mol is for the conversion at T7T12-model1. Although ΔE_{auto} in ZSM-5 is smaller than that in aqueous solution, still it is very high. From the obtained ΔE_{exch} and ΔE_{auto} , the exchange of bare Cu ion and autoreduction from bare Cu^{2+} would not be preferable at room temperature.

Department..... Chemistry..... Student's signature.....
Field of study..... Chemistry..... Advisor's signature.....
Academic year..... 2547.....

ACKNOWLEDGEMENT

I would like to affectionately give all gratitude to my family members, particularly, my bother “Mr. Atthapron Unjit” for their wholehearted understanding, encouragement, and support throughout my entire study.

Gratefully thanks to Associate Professor Dr. Sirirat Kokpol, Associate Professor Dr. Supot Hannongbua and Dr. Atticha Chaisuwan for their advice as thesis committee.

I also would like to acknowledge the Computational Chemistry Unit Cell (CCUC) for computing and other facilities.

I also would like to thanks Mr. Ugrid Poombub for providing ZSM-5 structures from preparation of them using Molecular Dynamic Simulation.

Finally, this thesis would never be completed without the excellent advice from my thesis advisor, Associate Professor Dr. Vudhichai Parasuk, who always provides me the useful guidance, suggestion, encouragement, and understanding during the whole research.



สถาบันวิทยบริการ
จุฬาลงกรณ์มหาวิทยาลัย

CONTENTS

	Pages
ABTRACT IN THAI	iv
ABTRACT IN ENGLISH	v
ACKNOWLEDGEMENT	vi
CONTENTS	vii
LIST OF FIGURES	xi
LIST OF TABLES	xiv
CHAPTER 1 INTRODUCTION	1
1.1 Research Rationale.....	1
CHAPTER 2 BACKGROUND	3
2.1 Zeolites.....	3
2.1.1 Structures of Zeolites.....	4
2.2 Application of Zeolites.....	7
2.2.1 Zeolites as Molecular Sieves.....	7
2.2.2 Zeolites as Ion Exchangers.....	7
2.2.3 Zeolites as Catalysts.....	8
2.3 ZSM-5.....	10
2.4 CuZSm-5 Zeolite Catalyst.....	11
2.5 Decomposition of Nitrogen Oxides (NO _x) in CuZSM-5 Zeolite Catalyst.....	11
2.6 Literature Review.....	13
2.7 Goals of This Study.....	14
CHAPTER 3 QUANTUM CHEMICAL CALCULATIONS	15
3.1 Classical and Quantum Mechanics.....	15
3.2 The time-dependent Schrödinger equation.....	16
3.3 The time-independent Schrödinger equation.....	16
3.4 The Born-Oppenheim Approximation.....	18
3.5 Molecular Orbital Theory.....	19

	Pages
3.6 The Hartree approximation.....	19
3.7 The Hartree-Fock Approximation.....	20
3.8 The Basis Set Approximation and Roothaan-Hall Equation.....	22
3.9 Basis Sets.....	27
3.9.1 Minimal Basis Set.....	29
3.9.2 Extended Basis Set.....	30
3.9.3 Polarization Basis Set.....	32
3.9.4 Diffuse Basis Set.....	32
3.10 Density Functional Theory (DFT).....	33
3.10.1 The Local Density Approximation.....	39
3.10.2 The Gradient Gradient Approximation	41
3.10.3 Hybrid Functional.....	44
CHAPTER 4 CALCULATIONS.....	45
4.1 Molecular Dynamic (MD) Simulation.....	45
4.1.1 Preparation of ZSM-5 Structure.....	45
4.2 Quantum Calculation.....	48
4.2.1 HZSM-5 Cluster Model.....	48
4.2.2 CuZSM-5 Cluster Model.....	49
4.2.3 Exchanged Energy.....	51
4.2.4 Autoreduction Energy.....	51
CHAPTER 5 RESULTS.....	52
5.1 HZSM-5.....	53
5.1.1 Optimized Structures of HZSM-5.....	53
5.1.1.1 T6T12.....	53
5.1.1.2 T8T8.....	54
5.1.1.3 T7T12-model1.....	55
5.1.1.4 T7T12-model2.....	56
5.2 One-ion Exchanged Cu ²⁺ ZSM-5.....	57
5.2.1 Optimized Structures of One-ion Exchanged Cu ²⁺ ZSM-5.....	57

	Pages
5.2.1.1 T6T12.....	57
5.2.1.2 T8T8.....	58
5.2.1.3 T7T12-model1.....	59
5.2.1.4 T7T12-model2.....	60
5.2.2 Exchanged Energy of One-ion Exchanged Cu ²⁺ ZSM-5.....	61
5.3 One-ion exchanged Cu ⁺ ZSM-5.....	62
5.3.1 Optimized Structures of One-ion Exchanged Cu ⁺ ZSM-5.....	62
5.3.1.1 T6T12.....	62
5.3.1.2 T8T8.....	64
5.3.1.3 T7T12-model1.....	66
5.3.1.4 T7T12-model2.....	68
5.3.2 Exchanged Energy of One-ion Exchanged Cu ⁺ ZSM-5.....	70
5.4 Two-ion exchanged Cu ⁺ ZSM-5.....	71
5.4.1 Optimized Structures of Two-ion Exchanged Cu ⁺ ZSM-5.....	71
5.4.1.1 T6T12.....	71
5.4.1.2 T8T8.....	73
5.4.1.3 T7T12-model1.....	75
5.4.1.4 T7T12-model2.....	77
5.4.2 Exchanged Energy of Two-ion Exchanged Cu ⁺ ZSM-5.....	79
5.5 Autoreduction Energy of Cu ²⁺ to Cu ⁺ in ZSM-5 at T6T12, T8T8, T7T12-model1, and T7T12-Model2.....	80
5.6 Combined Exchanged and Autoreduction Energy of Cu ²⁺ at T6T12, T8T8, T7T12-model1, and T7T12-model2 Exchanged Sites.....	81

	Pages
CHAPTER 6 DISCUSSIONS	82
6.1 Optimized Structures of HZSM-5.....	82
6.2 Optimized Structures of One-ion exchanged Cu^{2+} ZSM-5.....	82
6.3 Optimized Structures of One-ion exchanged Cu^+ ZSM-5.....	83
6.4 Optimized Structures of Two-ion exchanged Cu^+ ZSM-5.....	83
6.5 Exchanged Energy of CuZSM-5 at T6T12, T8T8, T7T12-model1, and T7T12-model2.....	84
6.6 Autoreduction of Cu^{2+} to Cu^+ in ZSM-5 at T6T12, T8T8, T7T12-model1, and T7T12-model2.....	84
CHAPTER 7 CONCLUSIONS	84
7.1 Optimized Structures of HZM-5 and CuZSM-5 Exchanged Sites.....	86
7.2 Exchanged Energy of Cu Species in ZSM-5 at Room Temperature.....	86
7.3 Autoreduction of Cu^{2+} to Cu^+ in ZSM-5 at T6T12, T8T8, T7T12-model1, and T7T12-model2 Exchanged Site at Room Temperature.....	87
REFERENCES	88
CURRICULUM VITAE	92

LIST OF FIGURES

Figures	Pages
2.1 An example of natural zeolite: (a) Mordenite (MOR) An example of synthetic zeolite: (b) Zeolite A (LTA).....	3
2.2 The linking of Primary building unit of $[\text{SiO}_4]^{4-}$ and $[\text{AlO}_4]^{5-}$ tetrahedra.....	4
2.3 The secondary building units (SBUs) recognized in zeolite frameworks; (a) single four ring (S4R), (b) single six ring (S6R), (c) single eight ring (S8R), (d) double four ring (D4R), (e) double six ring (D6R), (f) complex 4-1, (g) complex 5-1, and (h) complex 4-4-1.....	5
2.4 The combinations of β -cages produce several zeolites.....	6
2.5 Recovery of linear hydrocarbons from their mixtures by using zeolite A.....	7
2.6 Schematic of the cracking process which use zeolites as catalyst.....	8
2.7 Representation of (a) reactant shape selectivity in channel of zeolite A (rejection of branched chain hydrocarbons), (b) product shape selectivity in ZSM-5 channels (p-xylene diffuse preferentially out of the channels), (c) Transition state shape selectivity in mordenite channels (transition state B can be breakdown and diffuse out as 1, 2, 4-trimethylbenzene, but transition state A cannot).....	9
2.8 (a) The straight channels and sinusoidal channels of ZSM-5 (b) Si/Al tetrahedra comprise as 10-membered ring.....	12
2.9 (a) The structure of Cu^{2+} at T8T8 site was calculated by MD (b) The cluster model of Cu^{2+} at T8T8 site was optimized by MO.....	13
2.10 Vicinity of T sites that have most chance of attach of Cu species.....	14
3.1 A molecular coordinate system: i, j = electrons; A, B = nuclei.....	17
3.2 Illustration of SCF procedure.....	26
3.3 The approximation of STO by a set of several GTOs.....	29
3.4 Charge distribution of HCN molecule.....	31

Figures

3.5	$2p_z$ -function induces a polarization of 1s-orbital for H atom in HCN.....	32
4.1	Simulated HZSM-5 structure for Al-substitution at 4 exchanged sites: (a) HZSM-5(T6T12), (b) HZSM-5(T8T8), (c) HZSM-5(T7T12-model1), and (d) HZSM-5(T7T12-model1).....	47
4.2	Cluster models were obtained from the simulated HZSM-5 structure and then adjusted to the quantum calculations: (a) HZSM-5(T6T12), (b) HZSM-5(T8T8), (c) HZSM-5(T7T12-model1), and (d) HZSM-5(T7T12-model1).....	49
5.1	Optimized structures of HZSM-5(T6T12).....	53
5.2	Optimized structures of HZSM-5(T8T8).....	54
5.3	Optimized structures of HZSM-5(T7T12-model1).....	55
5.4	Optimized structures of HZSM-5(T7T12-model2).....	56
5.5	Optimized structures of one-ion exchanged Cu^{2+} ZSM-5.....	57
5.6	Optimized structures of one-ion exchanged Cu^{2+} ZSM-5.....	58
5.7	Optimized structures of one-ion exchanged Cu^{2+} ZSM-5.....	59
5.8	Optimized structures of one-ion exchanged Cu^{2+} ZSM-5.....	60
5.9	Optimized structures of one-ion exchanged Cu^+ ZSM-5(T6T12, Cu^+ at T6).....	62
5.10	Optimized structures of one-ion exchanged Cu^+ ZSM-5(T6T12, Cu^+ at T12).....	62
5.11	Optimized structures of one-ion exchanged Cu^+ ZSM-5(T8T8, Cu^+ at T8).....	64
5.12	Optimized structures of one-ion exchanged Cu^+ ZSM-5(T6T12, Cu^+ at T'8).....	64
5.13	Optimized structures of one-ion exchanged Cu^+ ZSM-5(T7T12-model1, Cu^+ at T7).....	66
5.14	Optimized structures of one-ion exchanged Cu^+ ZSM-5(T7T12-model1, Cu^+ at T12).....	66
5.15	Optimized structures of one-ion exchanged Cu^+ ZSM-5(T7T12-model2, Cu^+ at T7).....	68

Figures

5.16 Optimized structures of one-ion exchanged Cu^+ ZSM-5(T7T12-model2, Cu^+ at T12).....	68
5.17 Optimized structures of two-ion exchanged Cu^+ ZSM-5(T6T12).....	71
5.18 Optimized structures of two-ion exchanged Cu^+ ZSM-5(T8T8).....	73
5.19 Optimized structures of two-ion exchanged Cu^+ ZSM-5(T7T12-model1).....	75
5.20 Optimized structures of two-ion exchanged Cu^+ ZSM-5(T7T12-model2).....	77
7.1 The most favorable exchange; one-ion exchanged Cu^{2+} ZSM-5(T6T12).....	86

LIST OF TABLES

	Pages
Tables	
4.1 All possible substitutions for 2 Al in MFI.....	45
4.2 CuZSM-5 exchanged sites were optimized partially using B3LYP/6-31G(d,p).....	50
5.1 Cu ²⁺ -O distances of one-ion exchanged Cu ²⁺ ZSM-5(T6T12).....	51
5.2 Cu ²⁺ -O distances of one-ion exchanged Cu ²⁺ ZSM-5(T8T8).....	58
5.3 Cu ²⁺ -O distances of one-ion exchanged Cu ²⁺ ZSM-5(T7T12-model1)....	59
5.4 Cu ²⁺ -O distances of one-ion exchanged Cu ²⁺ ZSM-5(T7T12-model2)....	60
5.5 Exchanged energy of Cu ²⁺ exchanged in T6T12, T8T8, T7T12-model1, and T7T12-model2 exchanged site.....	61
5.6 Distances of Cu ⁺ -O and H ⁺ -O of one-ion exchanged Cu ⁺ ZSM-5(T6T12) when Cu ⁺ at T6 and T12 sites.....	62
5.7 Distances of Cu ⁺ -O and H ⁺ -O of one-ion exchanged Cu ⁺ ZSM-5(T8T8) when Cu ⁺ at T8 and T8' sites.....	65
5.8 Distances of Cu ⁺ -O and H ⁺ -O of one-ion exchanged Cu ⁺ ZSM-5(T7T12-model1) when Cu ⁺ at T7 and T12 sites.....	67
5.9 Distances of Cu ⁺ -O and H ⁺ -O of one-ion exchanged Cu ⁺ ZSM-5(T7T12-model2) when Cu ⁺ at T7 and T12 sites.....	69
5.10 Exchanged energy of one-ion exchanged Cu ⁺ ZSM-5 at T6T12, T8T8, T7T12-model1, and T7T12-model2 exchanged site.....	70
5.11 Cu ⁺ -O distances of two-ion exchanged Cu ⁺ ZSM-5(T6T12).....	72
5.12 Cu ⁺ -O distances of two-ion exchanged Cu ⁺ ZSM-5(T8T8).....	74
5.13 Cu ⁺ -O distances of two-ion exchanged Cu ⁺ ZSM-5(T7T12-model1).....	76
5.14 Cu ⁺ -O distances of two-ion exchanged Cu ⁺ ZSM-5(T7T12-model2).....	78
5.15 Exchanged energy of two-ion exchanged Cu ⁺ ZSM-5 at T6T12, T8T8, T7T12-model1, and T7T12-model2 exchanged site.....	79
5.16 Autoreduction energy of Cu ²⁺ in the cavity of ZSM-5 at T6T12, T8T8T7T12-model1, and T7T12-model2 exchanged site.....	80

Tables

5.17 Combined ΔE_{exch} and ΔE_{auto} of Cu^{2+} in ZSM-5 at T6T12, T8T8, T7T12-model1, and T7T12-model2 exchanged site.....	81
---	----



สถาบันวิทยบริการ
จุฬาลงกรณ์มหาวิทยาลัย

CHAPTER 1

INTRODUCTION

1.1 Research Rationale

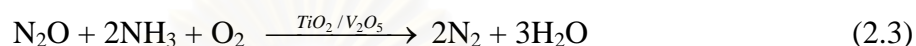
Zeolites are crystalline aluminosilicate mineral occurring naturally and synthetically. They have unique 3-D structures and possess excellent properties such as molecular sieves, ion exchangers, catalysts, etc.¹⁻³

By potential versatility of the zeolites, for many decades, researchers have been inspiring to investigate and develop either aspect of improvement their properties, and of utilities. Recently, zeolites have been developed to use in many industries. For examples; in detergent industry, use of zeolites as builder, instead polyphosphates, to exchange Ca^{2+} and Mg^{2+} from washing water to prevent their precipitation by surfactant molecules; based upon a molecular sieving action, n-paraffins can be separated from i-paraffins for use as feedstocks for detergent and chemical industry; in petrochemical industry, zeolites are used as catalysts in hydrocracking, isomerization, and alkylation.³ Usage of zeolites as catalysts is a major objective of their utilities and many researches in this aspect.

Because their high surface area, they indicate higher efficiency than other catalysts. Not only the zeolites are used as excellent catalysts in petrochemical industry, but also in environmental treatments.³ Example is the use of copper-exchanged ZSM-5 (CuZSM-5) as catalyst for decomposition of nitrogen oxides (NO_x), which was discovered by M. Iwamoto.¹⁷

The decomposition of NO_x is very interest reaction.⁴⁻¹⁷ NO_x exhaust causes environmental damages in form of air pollution and acid rain. If living things receive NO_x in high quantity and for long time, they can develop lung cancer and brain and nervous system damage.

The oxide forms of NO_x (NO, NO₂, N₂O) are the most difficult to eliminated from different combustion sources, such as, factories, power plants, and exhaust pipe of automobiles, etc. Recently, NO_x can be removed in the selective catalytic reduction (SCR) process using ammonia on TiO₂/V₂O₅ catalyst to convert NO_x to N₂ and H₂O in the exhaust.¹³



These systems are high efficiency, but the key problem is the storage of NH₃. Alternatively, CuZSM-5 catalyst can be used to convert NO_x with the use of more environmentally benign reductant (light hydrocarbon) for indirect decomposition of NO_x¹⁴ or without reductant for direct decomposition of NO_x.^{15,16}

CuZSM-5 can be prepared by exchanging with Cu²⁺ ion from copper chloride (CuCl₂) or copper acetate (Cu(CH₃COO)₂) or copper propionate (Cu(C₂H₅COO)₂) solutions.⁷ Then calcined at 400°C. Cu⁺ ions were found after the calcinations. Experiments also found that activity of CuZSM-5 depends on numbers of Cu⁺ ions in ZSM-5. However, the characterization of copper active sites, the autoreduction of Cu²⁺ to Cu⁺ in the cavity of ZSM-5 and the mechanism of NO_x decomposition are still unknown. Goals of this study are to find preferable exchanged Cu species (Cu as Cu²⁺ and Cu⁺) and exchanged sites in the cavity of ZSM-5, and the autoreduction process of Cu²⁺ZSM-5 to Cu⁺ZSM-5 at low copper loading.

สถาบันวิทยบริการ
จุฬาลงกรณ์มหาวิทยาลัย

CHAPTER 2

BACKGROUND

2.1 Zeolites

Zeolite minerals were first discovered by Cronstedt in Sweden in 1756.¹ Since then, about 50 zeolite natural species have been discovered, and more than 100 species have been synthesized in the laboratory. Examples of natural and synthetic zeolites are given in Fig. 2.1.

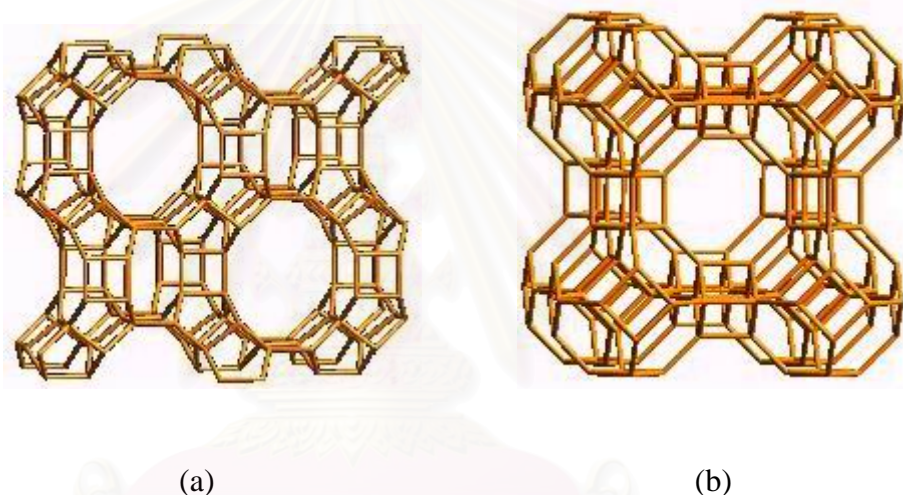


Fig. 2.1 An example of natural zeolite: (a) Mordenite (MOR)
An example synthetic zeolite: (b) Zeolite A (LTA).²

Zeolites are aluminosilicate minerals occurring naturally and synthetically. Their well-defined structures are 3-D framework of microporous inorganic crystalline solids. Generally their framework consists of primary building unit of $[\text{SiO}_4]^{4-}$ and $[\text{AlO}_4]^{5-}$ tetrahedra, as shown in Fig.2.2. All of the oxygen atoms in the tetrahedral are mutually linked to enclose micropores running throughout the framework that lead to an open structures.

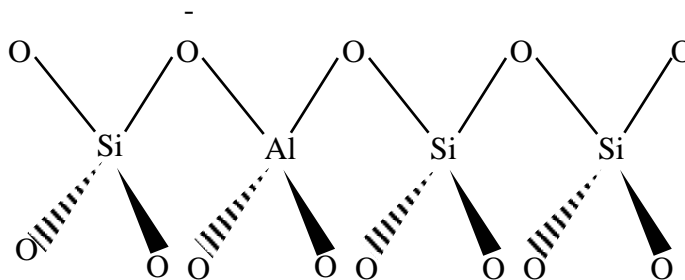


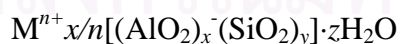
Fig. 2.2 The linking of primary building unit of $[\text{SiO}_4]^{4-}$ and $[\text{AlO}_4]^{5-}$ tetrahedra.¹

The appearance of the micropores may be cages, channels and/or cavities with the diameter is about 1-20 Å in which are filled with exchangeable cations, a certain amount of water and/or other molecules.

2.1.1 Structures of Zeolites

As mentioned, all zeolites have three-dimensional framework constructed by joining together $[\text{SiO}_4]^{4-}$ and $[\text{AlO}_4]^{5-}$ coordination polyhedra. The substitution of Al^{3+} into some of Si^{4+} produces a deficiency in electrical charge that must be locally neutralized by the presence of an additional positive ion (monovalent and divalent cations, such as Na^+ , Cu^+ , Ag^+ , Mg^{2+} , Cu^{2+} , etc.) within the interstices of the framework. However, according to Lowensteins' rule, the linking between two Al-tetrahedral units is forbidden because repulsion between the two negative charges of $\equiv\text{Al}-\text{O}^--\text{Si}\equiv$ sites. Different types of zeolites result from difference in the way of linking of tetrahedral and from the types of difference ions that substitute within the interstices.

The general formula for zeolites can be expressed as:



where $[(\text{AlO}_2)_x(\text{SiO}_2)_y]$ represents the framework atoms.

M^{n+} represents the cations M that $n = 1, 2$.

x, y, z represent the number of Al-, Si-tetrahedral and water molecules, respectively.

The extent and location of the water molecules which held in the interstices of the zeolite framework depends on the size and shape of the cavities and channels present, and the number and nature of the cations in the structure.

The linking of primary building tetrahedral $(\text{Si,Al})\text{O}_4$ give rise to secondary building units (SBUs) which is important for the classification of zeolite structures. The main SBUs of zeolite are shown in Fig 2.3. These denote only the aluminosilicate skeleton and exclude consideration of the cations and water molecules within the channels and cavities of the framework.

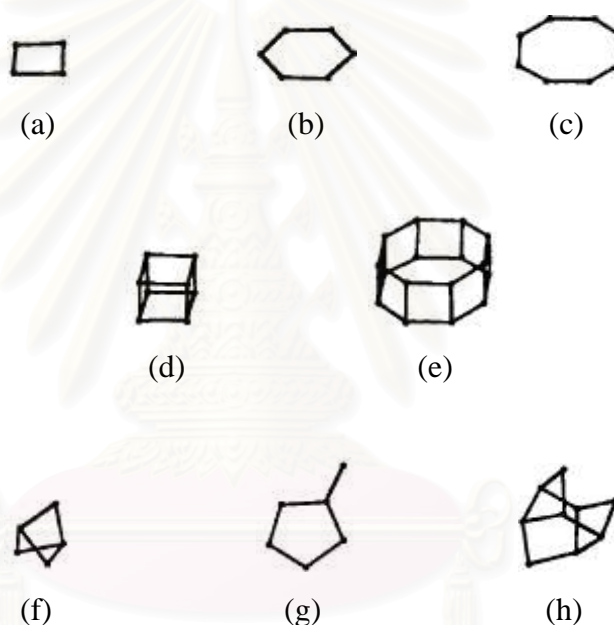


Fig. 2.3 The secondary building units (SBUs) recognized in zeolite frameworks; (a) single four ring (S4R), (b) single six ring (S6R), (c) single eight ring (S8R), (d) double four ring (D4R), (e) double six ring (D6R), (f) complex 4-1, (g) complex 5-1, and (h) complex 4-4-1.³

The joining of the SBUs to create the infinite lattice occur the rings containing 8, 10 or 12 linked tetrahedral, which are important to the zeolite structural features. For example, SBUs combines between β -cages in zeolite A are D4R.

The zeolite framework can be considered in terms of large polyhedral building blocks forming characteristic cages, such as the truncated octahedron (β -cages). The β -cages formed have an internal diameter of about 6 Å which is sufficient to encapsulate small molecules. Moreover, the combination of β -cages produces several zeolites (Fig. 2.4) with different sizes and shapes of cavities which utilize to their application in industries.

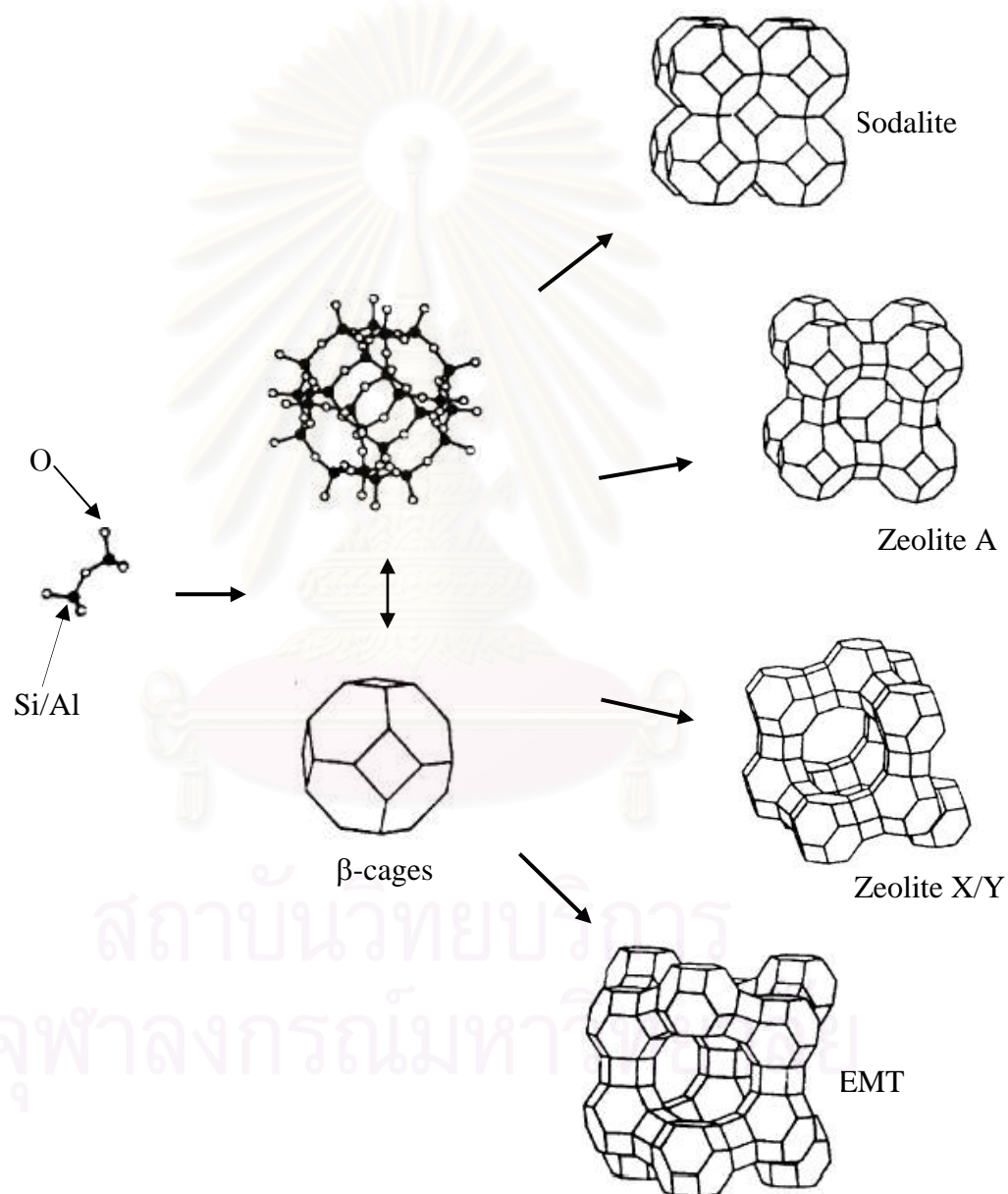


Fig. 2.4 The combinations of β -cages produce several zeolites.¹

2.2 Application of Zeolites

By characteristic architecture of zeolites, their three-dimensional framework comprises of a variety of internal channels and cavities with diameter are about 1-20 Å which enough to locate cation, water and other molecules. Therefore, they have the excellent properties, e.g., molecular sieve, ion exchanger, and catalyst.³ Consequently, both synthetic and natural zeolites can be applied into industries. The examples of zeolite applications as follows:

2.2.1 Zeolites as Molecular Sieves

The use of zeolites as “molecular sieve” is the first commercial success. The zeolites can selectively take up some molecules into cavities and rejecting others on the basis of their large effective molecular dimensions. Example of this is the use of zeolite A to recover linear hydrocarbons from mixtures with branched and cyclic hydrocarbons as shown in Fig. 2.5.

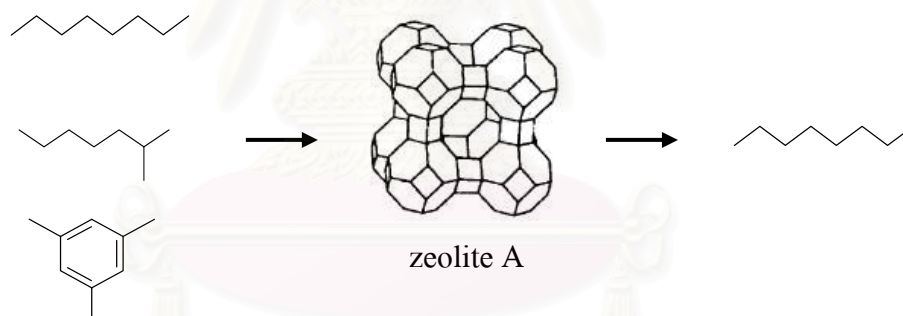


Fig. 2.5 Recovery of linear hydrocarbons from their mixtures by using zeolite A.³

2.2.2 Zeolites as Ion Exchangers

The use of zeolites as “ion exchangers” has been taken place to modify the catalytic on molecular sieving action of the parent zeolites. The cations held in their aluminosilicate anion framework are replaced by ion present in external solutions. Examples of this application are; the use of mixtures of zeolite A and zeolite X in the detergent industry as being the most effective builders to compensate the use of harmful chemical Sodium tri-polyphosphate (STPP) which can cause eutrophication of surface water with excessive formation of algae and subsequent oxygen deficiency,

the use of clinoptilolite and synthetic zeolite F in removing ammonium ion from waste water, etc.

2.2.3 Zeolites as Catalysts

Zeolites can be made as “catalysts” on the basis of their high surface areas. Since the last 40 years, the major employment of zeolites in this aspect is as acid cracking catalysts with over 99 % of the world’s petro production from crude oils. In cracking process, zeolite X (faujasite) is used to breakdown the long chain hydrocarbons where the major products of C_1 - C_3 gas, gasoline, light cycle oil, heavy gas oil and recycle oil are obtained. The schematic of this process is shown in Fig. 2.6.

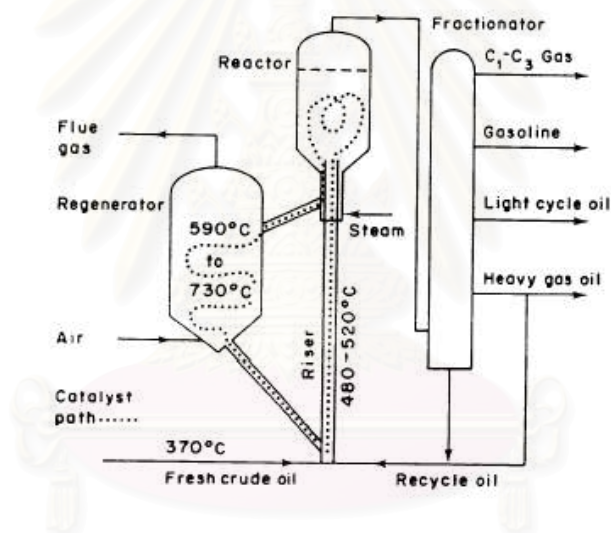


Fig. 2.6 Schematic of the cracking process that uses zeolites as catalyst.³

Several zeolites are used as shape-selective catalysts (Fig 2.7). Furthermore, ZSM-5 zeolite is used in dewaxing, benzene alkylation, and methanol to gasoline conversion (MTG) processes.

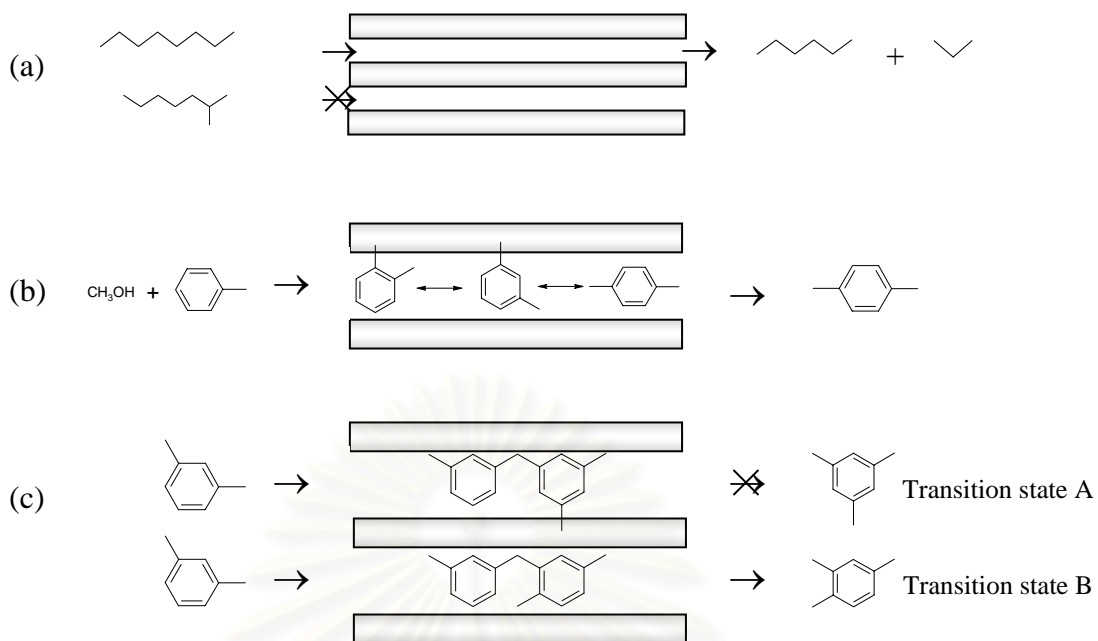


Fig. 2.7 Representation of (a) reactant shape selectivity in channel of zeolite A (rejection of branched chain hydrocarbons), (b) product shape selectivity in ZSM-5 channels (p-xylene diffuse preferentially out of the channels), (c) Transition state shape selectivity in mordenite channels (transition state B can be breakdown and diffuse out as 1, 2, 4-trimethylbenzene, but transition state A cannot).³

Besides the application of zeolites in the petrochemical aspect, they are also used as excellent catalyst in environmental treatments.³ For instance, exhaust gases (e.g., carbon monoxide (CO), nitrogen oxides (NO_x), sulfur dioxide (SO₂), etc.) that cause of air pollution can be minimized by using zeolites as catalyst.

สถาบันวิทยบริการ
จุฬาลงกรณ์มหาวิทยาลัย

2.3 ZSM-5

ZSM-5 is an important of the pentasil class of zeolites consists of a 3-D network of SiO_4 and AlO_4 tetrahedra.⁴ ZSM-5 is a highly siliceous material, one unit cell includes 96 tetrahedra and at most 8 of these can be Al. Tetrahedra are linked in such a way that they enclose channels and/or cavities. Their structure is very open with an internal volume of 0.17 ml/g. or 30 %. The lattice density is 1.7 g/ml. There are two types of channels as the straight channels (5.1, 5.6 Å) running perpendicular to sinusoidal channels (5.1, 5.4 Å).^{5, 6} The illustrations of ZSM-5 structure are shown in Fig 2.8a.

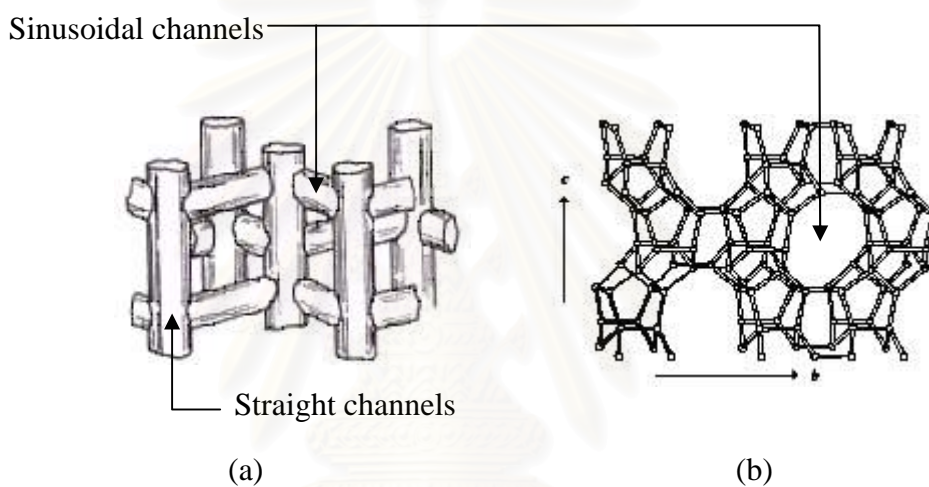


Fig. 2.8 (a) The straight channels and sinusoidal channels of ZSM-5
(b) Si/Al tetrahedra comprise as 10-membered ring.³

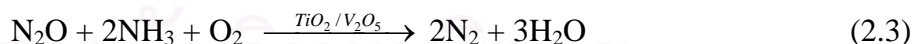
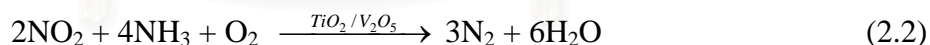
A channel intersection can be considered as a cavity that can be entered from 4 sides. Each entrance consists of a 10-membered ring. (Fig 2.8b) The compensating negative charges are in the form of cations located near Al.

2.4 CuZSM-5 Zeolite Catalyst

CuZSM-5 is stood for copper ion-exchanged ZSM-5 zeolite. CuZSM-5 can be prepared by exchanging, Sodium ion (Na^+) in the cavities of ZSM-5 (NaZSM-5) are exchanged with Cu from copper chloride (CuCl_2) or copper acetate ($\text{Cu}(\text{CH}_3\text{COO})_2$) or copper propionate ($\text{Cu}(\text{C}_2\text{H}_5\text{COO})_2$) solutions.⁷ Physical characterization of CuZSM-5⁸⁻¹⁰ suggests that most of the copper is present as isolated cations. In freshly exchanged CuZSM-5, all of Cu is present as Cu^{2+} species. Presumably as in the framework of ZSM-5, Cu^{2+} associated with pairs of $\equiv\text{Al-O}^-\text{Si}\equiv$ sites located in close proximity. Heating freshly CuZSM-5 results in Cu^{2+} reduce to Cu^+ cations. This process referred to as autoreduction. The locations of copper in channels produce active site which suitable as catalytic center for many reactions.¹¹

2.5 Decomposition of Nitrogen Oxides (NO_x) in CuZSM-5 Zeolite Catalyst

The oxide forms of nitrogen oxides (NO , NO_2 , $\text{N}_2\text{O} \rightarrow \text{NO}_x$) are some of the most difficult to eliminated from combustion sources. Catalytic systems have been investigated to address this problem.¹² Up to now, the most active commercial catalytic system is the selective catalytic reduction (SCR) using ammonia on $\text{TiO}_2/\text{V}_2\text{O}_5$ catalyst to convert NO_x to N_2 and H_2O in the exhaust.¹³



These systems are high efficiency, but the key problem is difficult of storing ammonia. In addition, if conversion is not complete, ammonia can be released to the atmosphere, which causes a problem worse than the release of NO_x . Consequently, catalysts that will convert NO_x using a more readily available, more environmentally benign reductant are needed.

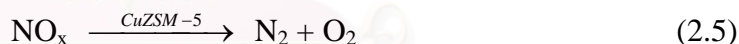
One of the most promising is a metal-exchanged form of ZSM-5 zeolite catalyst, particularly, CuZSM-5 which shows a significant ability to reduce NO_x. It is generally accepted that both Cu²⁺ and Cu⁺ species play an important role in NO_x decomposition.⁸ Comparison of the activity of this catalyst with that of Cu exchanged into other zeolites and other metals exchanged into ZSM-5 indicates that the high activity of CuZSM-5 results from the combined properties of the metal cation and the zeolite.

However, CuZSM-5 catalyst has high selectivity for both indirect and direct decomposition of NO_x.

The indirect decomposition of NO_x¹⁴ uses light hydrocarbons as reducing agent in CuZSM-5 catalyst to convert NO_x to N₂ and CO₂. For example; using CuZSM-5 is active above 300 °C with C₃H₆,



Direct decomposition of NO_x¹⁵⁻¹⁶ uses CuZSM-5 as catalyst to decompose NO_x to N₂ and O₂ without any reducing agent. This reaction was discovered by Iwamoto et al. and co-worker in 1986¹⁷ and can be expressed as



Although these systems have a high potential, a major disadvantage is that the performance of ZSM-5 under typical conditions for NO_x removal is inadequate to meet expected requirement. High moisture content in the exhaust streams renders the catalyst inactive. Moreover, thermal instability of ZSM-5, a narrow range of temperatures associated with optimal performance, and the effects of engine operation leading to varying emission of hydrocarbons and nitrogen oxides preclude the ZSM-5 catalytic systems from commercial viability. However, the characterization of copper active sites, the autoreduction of Cu²⁺ to Cu⁺ in the cavity of ZSM-5 and the mechanism of NO_x decomposition are still unknown, and should be investigated in order to increase possibility of development CuZSM-5 zeolite catalyst for NO_x decomposition to commercial viability. However, the grasp of the Cu species in this catalyst should therefore be a first step toward understanding the reaction mechanism.

2.6 Literature Review

In experimental studies, presumably as, in freshly exchanged CuZSM-5, active sites are vicinity of Cu^{2+} species that associated with pairs of $\equiv\text{Al-O}^-\text{Si}\equiv$ sites located in close proximity.⁸

In theoretical studies, active site structures of CuZSM-5 were investigated by Molecular Dynamic (MD) Simulations and Molecular Orbital (MO) calculations.¹¹ For MD simulations, 23 possible pairs of Al substitutions, which satisfy Lowenstein's rule, were determined. The results shown that coordination of Cu^{2+} at T8T8 site in 6-T ring was the lowest energies of all considered models. For MO Calculations with LANL2MB basis sets were also performed on cluster models based on the simulated T8T8 site. The structure of Cu^{2+} at T8T8 site was calculated by MD and the cluster model was then optimized by MO calculations are shown in Fig.2.9.

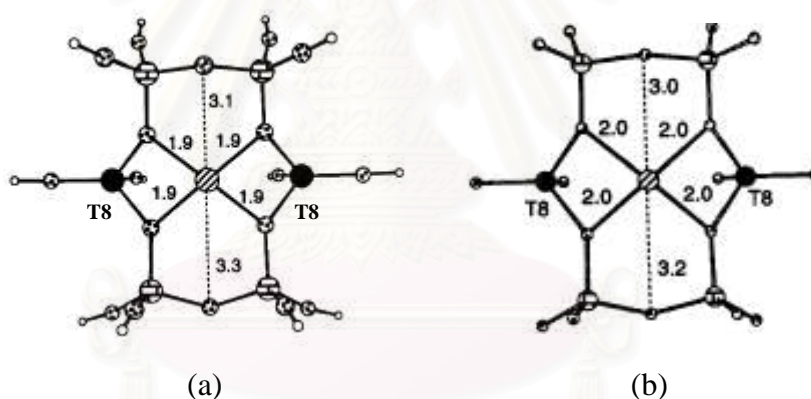


Fig. 2.9 (a) The structure of Cu^{2+} at T8T8 site was calculated by MD.

(b) The cluster model of Cu^{2+} at T8T8 site was optimized by MO.¹¹

In addition to T8T8 site, other Al substitutions in 6-T ring were also considered as lowest energy group such as T11T11, T7T12 site. Moreover, T5T12, and T6T12 site in 5-T ring was considered as the second lowest energy group following the 6-T ring.

2.7 Goals of This study

In the present study, density functional calculation is used to determine the structures and exchanged energy of Cu^{2+} and Cu^+ species, which are exchanged in the cavity of ZSM-5 at low copper loading. Moreover, the autoreduction of Cu^{2+} to Cu^+ are investigated and compared between their progresses in aqueous solution and in the cavity of ZSM-5. All calculations have been performed in vicinity of cavity called “T site” that have most chance of attach of Cu species.¹¹ These T sites are T6T12, T8T8, and T7T12.

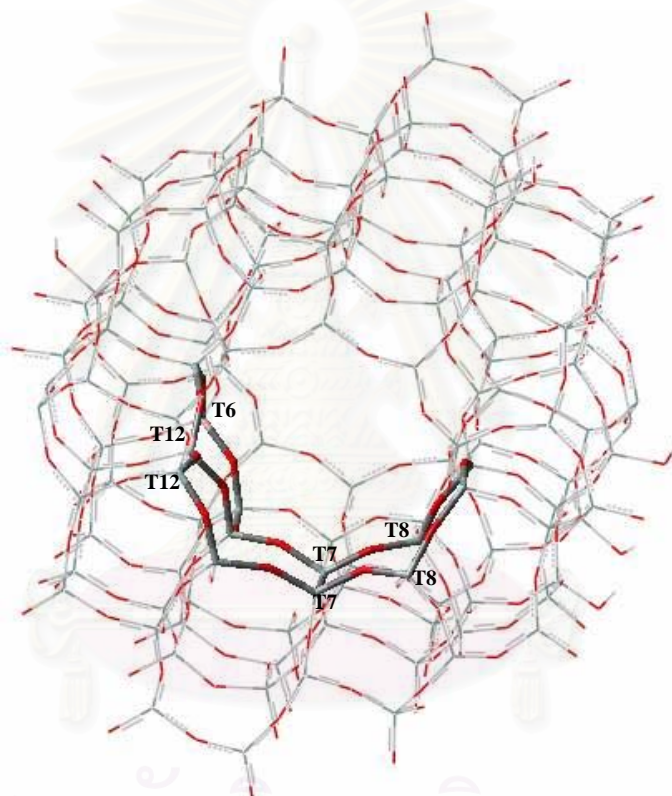


Fig. 2.10 Vicinity of T sites that have most chance of attach of Cu species.

The results of this study may describe more explicitly to the autoreduction of Cu species, which bring to understand in NO_x decomposition.

CHAPTER 3

QUANTUM CHEMICAL CALCULATIONS

3.1 Classical and Quantum Mechanic¹⁸⁻²¹

The most molecular behavior can be understood on the basis of one unified concept as “the Schrödinger equation”. Energy and many properties of a stationary state of a molecule can be obtained by the solution of the Schrödinger equation.

$$\hat{H}\Psi = E\Psi \quad (3.1)$$

where the Hamiltonian operator, \hat{H} , must be Hermitian. E is the eigenvalue representing the energy of state, and Ψ is the wavefunction.

The classical Hamiltonian or the total energy of a single particle moving in one dimension is the sum of the kinetic energy (T) and the potential energy (V)

$$\begin{aligned} H = E = T + V \\ = \frac{p^2}{2m} + V \end{aligned} \quad (3.6)$$

where p is momentum, m is mass.

In quantum mechanics, the electrons are characterized as wave-particle duality. Wavefunction are brought to better description of electronic behavior instead the classical equation. Energy of a molecule can be obtained by the solution of the Schrödinger wave equation.

3.2 The time-dependent Schrödinger equation¹⁸⁻²¹

In making the transition to a wave equation, physical variables in classical mechanics take the form of “operator”, in (3.6), $p \rightarrow \frac{\hbar}{i} \frac{\partial}{\partial x}$ and $x \rightarrow x$. Thus, the classical Hamiltonian can be rewritten in three dimensions as the Hamiltonian operator

$$\hat{H} = -\frac{\hbar^2}{2m} \left(\frac{\partial^2}{\partial x^2} + \frac{\partial^2}{\partial y^2} + \frac{\partial^2}{\partial z^2} \right) + V \quad (3.7)$$

where h is plank's constant, \hbar is Dirac's constant representing $h/2\pi$.

Thus, “the time-dependent Schrödinger equation” can be given as

$$\left(-\frac{\hbar^2}{2m} \left(\frac{\partial^2}{\partial x^2} + \frac{\partial^2}{\partial y^2} + \frac{\partial^2}{\partial z^2} \right) + V \right) \Psi = \frac{\hbar}{i} \frac{\partial \Psi}{\partial t} \quad (3.8)$$

or

$$\hat{H}\Psi = \frac{\hbar}{i} \frac{\partial \Psi}{\partial t} \quad (3.9)$$

3.3 The time-independent Schrödinger equation¹⁸⁻²¹

In the special circumstance where the Hamiltonian is independent of time, the wavefunction in (3.9) is written as a product of a spatial and temporal part,

$$\Psi(x, t) = \psi(x)e^{-iEt/\hbar} \quad (3.10)$$

substitute (3.10) into (3.9)

$$\hat{H}(\psi(x)e^{-iEt/\hbar}) = i\hbar \frac{\partial}{\partial t} (\psi(x)e^{-iEt/\hbar}) \quad (3.11)$$

Thus, the time-independent Schrödinger equation is given as

$$\hat{H}\psi = E\psi \quad (3.12)$$

For molecular system such as H_2 , the total Hamiltonian operator consists of kinetic (\hat{T}) and potential (\hat{V}) energy for all nuclei and electrons.

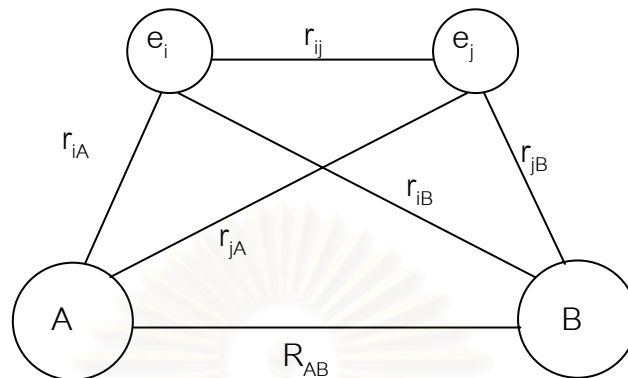


Fig. 3.1 A molecular coordinate system: i, j = electrons; A, B = nuclei.

Thus,

$$\hat{H}_{\text{tot}} = \hat{T}_N + \hat{T}_e + \hat{V}_{Ne} + \hat{V}_{ee} + \hat{V}_{NN} \quad (3.13)$$

in atomic unit (a.u.);

$$\hat{H}_{\text{tot}} = -\sum_{A=1}^N \frac{1}{2M_A} \nabla_A^2 - \sum_{i=1}^n \frac{1}{2} \nabla_i^2 - \sum_{A=1}^N \sum_{i=1}^n \frac{Z_A}{r_{iA}} + \sum_{i=1}^n \sum_{j>i}^n \frac{1}{r_{ij}} + \sum_{A=1}^N \sum_{B>A}^N \frac{Z_A Z_B}{R_{AB}} \quad (3.14)$$

where the Laplacian operators ∇^2 involve differentiation with respect to the coordinates of the particle in the system. A and B refer to nuclei with atomic numbers Z_A and Z_B , respectively. i and j refer to electrons. M is the ratio of the mass of nucleus to the mass of an electron. N is the number of nucleus and n is the number of electrons. The first and second term is the operator for the kinetic energy of the nuclei and electrons, respectively. The third term is the nuclear-electron attraction where r_{iA} being the distance between electron i and nucleus A . The fourth term is the electron-electron repulsion where r_{ij} being the distance between electrons i and j . The last term is the nuclear-nuclear repulsion where R_{AB} being the distance between nuclei A and B .

3.4 The Born-Oppenheimer Approximation¹⁸⁻²¹

The Born-Oppenheimer Approximation is applied to reduce the complexity of the Schrödinger equation. Since nuclei are much heavier than electrons, they move more slowly. Thus, the electrons in a molecule can be considered as moving in the field of fixed nuclei. The kinetic energy of the nuclei can be neglected and the nuclear-nuclear repulsion can be considered to be constants.

Thus, \hat{H}_{tot} in (3.13) is reduced as “electronic Hamiltonian operator”, which can be expressed as

$$\begin{aligned}\hat{H}^{\text{el}} &= \hat{T}_e + \hat{V}_{\text{Ne}} + \hat{V}_{ee} \\ &= -\sum_{i=1}^n \frac{1}{2} \nabla_i^2 - \sum_{A=1}^N \sum_{i=1}^n \frac{Z_A}{r_{iA}} + \sum_{i=1}^n \sum_{j>i}^n \frac{1}{r_{ij}}\end{aligned}\quad (3.15),$$

and “Electronic Schrödinger equation” can be given as

$$\hat{H}^{\text{el}} \Psi^{\text{el}} = E^{\text{eff}} \Psi^{\text{el}} \quad (3.16)$$

where Ψ^{el} is the electronic wave function, and E^{eff} is the effective electronic energy which depends on the relative nuclear coordinates, R .

The constant nuclear-nuclear repulsion has no effect on the operator eigenfunctions and only adds to the operator eigenvalue. They must also be included with electronic energy to obtain the total energy.

$$E_{\text{tot}} = E^{\text{eff}} + \sum_A \sum_{B>A}^N \frac{Z_A Z_B}{R_{AB}} \quad (3.17)$$

The deficiency of the Born-Oppenheimer Approximation occurs when the energy of over a solution to Schrödinger equation comes close to each other. However, this approximation is usually very good and introduces only very small errors, an accuracy of 10^{-4} a.u.

3.5 Molecular Orbital Theory¹⁸⁻²¹

Molecular orbital theory is an approach, which uses one-electron functions or orbitals to approximate the full wavefunction. The molecular orbital, $\chi(x, y, z)$ is a function of the Cartesian coordinates of a single electron. $|\psi|^2$ is interpreted as the probability distribution of the electron in space. To describe the distribution of an electron completely, the dependence on the spin coordinates (ω) also has to be included. Values of the ω may be $+1/2$ or $-1/2$. In the presence of an external magnetic field, the spin aligned along the field corresponding to spin up, $\alpha(\omega)$ and the spin aligned opposite the field corresponding to spin down, $\beta(\omega)$. Thus,

$$\alpha(+1/2) = 1 \quad \alpha(-1/2) = 0 \quad (3.18)$$

$$\beta(+1/2) = 0 \quad \beta(-1/2) = 1 \quad (3.19)$$

The complete wavefunction for a single electron is the product of a molecular orbital and a spin function, $\chi(\mathbf{r})\alpha(\omega)$ or $\chi(\mathbf{r})\beta(\omega)$.

It is termed a spin orbital; $\chi(\mathbf{r}, \omega)$

3.6 The Hartree approximation¹⁸⁻²¹

“The Hartree approximation” proposed the simplest way to approximate an n-electron system, their wavefunction can be described as a product of spin orbitals which is called “Hartree product”,

$$\Psi_{\text{HP}}(\mathbf{r}_1 s_1, \mathbf{r}_2 s_2, \dots, \mathbf{r}_n s_n) = \frac{1}{\sqrt{N}} \chi_1(\mathbf{r}_1 s_1) \chi_2(\mathbf{r}_2 s_2) \dots \chi_n(\mathbf{r}_n s_n) \quad (3.20)$$

where N is normalization constant.

However, the Hartree approximation does not account for exchange interactions since (3.20) does not satisfy anti symmetry principle.

3.7 The Hartree-Fock Approximation¹⁸⁻²¹

The exchange interaction can be rectified by “Hartree-Fock approximation”, which the wavefunction is written as an antisymmetrized product of orbitals. Pauli Exclusion Principle state that “It is not possible for a molecular orbital to be occupied by two electrons of the same spin” is required to obtain antisymmetry property of wavefunction. The coordinates of electrons i and j are interchanged, then, the product $\dots\chi_i(\mathbf{r}_i s_i)\dots\chi_j(\mathbf{r}_j s_j)\dots$ become $\dots\chi_i(\mathbf{r}_j s_j)\dots\chi_j(\mathbf{r}_i s_i)\dots$. Thus, the Hartree-Fock (HF) wavefunction amounts to a linear combination of the terms in (3.20);

$$\begin{aligned} \Psi_{\text{HF}}(\mathbf{r}_1 s_1, \mathbf{r}_2 s_2, \dots, \mathbf{r}_n s_n) \\ = \frac{1}{\sqrt{N!}} [\chi_1(\mathbf{r}_1 s_1)\chi_2(\mathbf{r}_2 s_2)\dots\chi_n(\mathbf{r}_n s_n) - \chi_1(\mathbf{r}_2 s_2)\chi_2(\mathbf{r}_1 s_1)\dots\chi_n(\mathbf{r}_n s_n) + \dots] \end{aligned} \quad (3.21)$$

or

$$= \frac{1}{\sqrt{N!}} \sum_p (-1)^p \hat{P}[\chi_1(\mathbf{r}_1 s_1)\chi_2(\mathbf{r}_2 s_2)\dots\chi_n(\mathbf{r}_n s_n)] \quad (3.22)$$

where \hat{p} is a permutation operator, changing the coordinates $1, 2, \dots, n$ according to any of the $n!$ possible permutations among the n electrons. $(-1)^p$ is $+1$ or -1 for even and odd permutations.

To fulfil (3.22), the HF wavefunction can be efficiently represented as an $n \times n$ determinant, known as Slater determinant,²⁰

$$\Psi_{\text{HF}} = \frac{1}{\sqrt{N!}} \begin{vmatrix} \chi_1(\mathbf{r}_1 s_1) & \chi_1(\mathbf{r}_2 s_2) & \dots & \chi_1(\mathbf{r}_n s_n) \\ \chi_2(\mathbf{r}_1 s_1) & \chi_2(\mathbf{r}_2 s_2) & \dots & \chi_2(\mathbf{r}_n s_n) \\ \vdots & \vdots & \ddots & \vdots \\ \chi_n(\mathbf{r}_1 s_1) & \chi_n(\mathbf{r}_2 s_2) & \dots & \chi_n(\mathbf{r}_n s_n) \end{vmatrix} \quad (3.23)$$

where the orbitals are subject to the orthonormal constraint,

$$\int \psi_i^*(\mathbf{r})\psi_j(\mathbf{r})d\mathbf{r} = \langle \psi_i | \psi_j \rangle = \delta \quad (3.24)$$

Thus, the Slater determinant can also be written as,

$$\Psi_{\text{HF}} = \frac{1}{\sqrt{N!}} |\chi_1(r_1, s_1) \chi_2(r_2, s_2) \cdots \chi_n(r_n, s_n)\rangle \quad (3.25)$$

The HF energy can be evaluated by taking the expectation value of the Hamiltonian or called Fock operator (3.15) with the Slater determinant,

$$\begin{aligned} E_{\text{HF}} &= \langle \Psi_{\text{HF}} | \mathbf{F} | \Psi_{\text{HF}} \rangle \\ &= \sum_{i=1}^n \int \chi_i^*(r_i) \left(-\frac{1}{2} \nabla^2 + v_{\text{ext}}(r_i) \right) \chi_i(r_i) dr_i + \frac{1}{2} \sum_{i=1}^n \sum_{j=1}^n \iint \frac{|\chi_i(r_i)|^2 |\chi_j(r_j)|^2}{|r_i - r_j|} dr_i dr_j \\ &\quad - \frac{1}{2} \sum_{i=1}^n \sum_{j=1}^n \iint \frac{\chi_i^*(r_i) \chi_i(r_j) \chi_j^*(r_j) \chi_j(r_i)}{|r_i - r_j|} \delta_{ij} dr_i dr_j \end{aligned} \quad (3.26)$$

or

$$\begin{aligned} E_{\text{HF}} &= \sum_{i=1}^n [i|h|i] + \frac{1}{2} \sum_{i=1}^n \sum_{j=1}^n [ii|jj] - \frac{1}{2} \sum_{i=1}^n \sum_{j=1}^n [ij|ji] \\ &= \sum_{i=1}^n h_{ii} + \frac{1}{2} \sum_{i=1}^n \sum_{j=1}^n J_{ij} - \frac{1}{2} \sum_{i=1}^n \sum_{j=1}^n K_{ij} \end{aligned} \quad (3.27)$$

where $v_{\text{ext}}(r_i)$ is the HF mean field potential, which two electron interaction is described as an average one electron interaction, i.e. the interaction experienced by the i^{th} electron in the presence of all other electrons, h_{ii} is one-electron operator; J_{ij} is coulomb operator, and K_{ij} is exchange operator.

According to the variational principle, the best spin orbitals are those that give the lowest possible HF energy.

For closed-shell restricted HF wavefunction, the spin orbitals are constrained to have the same spatial function for α and β spin functions and the molecular states are allowed to have only an even number N of electrons, with all electrons paired such that $n = N/2$ spatial orbitals are doubly occupied. Then,

$$|\Psi_{\text{HF}}\rangle = |\chi_1 \chi_2 \chi_3 \chi_4 \cdots \chi_{n-1} \chi_n\rangle = |\psi_1 \bar{\psi}_1 \psi_2 \bar{\psi}_2 \cdots \psi_{n/2} \bar{\psi}_{n/2}\rangle \quad (3.28)$$

where ψ_i represents the spatial orbital or molecular orbital (MO) while bar and unbar term represents β spin and α spin, respectively.

Thus, the energy E_{HF} can be given as

$$\begin{aligned}
 E_{\text{HF}} &= 2 \sum_i^{n/2} \int \psi_i^*(\mathbf{r}_i) \left(-\frac{1}{2} \nabla^2 + v_{\text{ext}}(\mathbf{r}_i) \right) \psi_i(\mathbf{r}_i) d\mathbf{r}_i + \sum_{i=1}^{n/2} \sum_{j=1}^{n/2} 2 \iint \frac{|\psi_i(\mathbf{r}_i)|^2 |\psi_j(\mathbf{r}_j)|^2}{|\mathbf{r}_i - \mathbf{r}_j|} d\mathbf{r}_i d\mathbf{r}_j \\
 &\quad - \sum_{i=1}^{n/2} \sum_{j=1}^{n/2} \iint \frac{\psi_i^*(\mathbf{r}_i) \psi_i(\mathbf{r}_j) \psi_j^*(\mathbf{r}_j) \psi_j(\mathbf{r}_i)}{|\mathbf{r}_i - \mathbf{r}_j|} \delta_{ij} d\mathbf{r}_i d\mathbf{r}_j \\
 &= 2 \sum_{i=1}^{n/2} (\mathbf{i} | \mathbf{h} | \mathbf{i}) + \sum_{i=1}^{n/2} \sum_{j=1}^{n/2} 2(\mathbf{ii} | \mathbf{jj}) - (\mathbf{ij} | \mathbf{ji}) \\
 &= 2 \sum_{i=1}^{n/2} h_{ii} + \sum_{i=1}^{n/2} \sum_{j=1}^{n/2} (2J_{ij} - K_{ij}) \tag{3.29}
 \end{aligned}$$

The last term is of significant interest since it arises from the antisymmetric nature of the HF wavefunction, it vanishes when $i = j$, which is an artifact of the Pauli principle. Consequently this term is called the exchange energy, E_{xc} . It should also be noted that in practice an extra term due to the repulsion energy between the ions must be added to (3.29) in order to obtain the total energy of the system.

In general the HF equations cannot be solved analytically. They are solved using an iterative process known as the self-consistent field procedure.²² Since the desired orbitals also make up their one-electron effective potential, the set of orbitals that give rise to the same after solving HF equation are known as the self-consistent orbitals, and they are the groundstate orbitals for that system within the HF approximation. The self-consistent field procedure²² starts with an initial guess for the orbitals, and successive iterations are performed with new orbitals until the self-consistent condition is achieved.

3.8 The Basis Set Approximation and Roothaan-Hall equation¹⁸⁻²¹

The partial molecular orbitals is expanded as linear combination of a set of known one-electron function φ_μ , known as basis functions.

$$\psi_i = \sum_{\mu=1}^k C_{\mu i} \varphi_\mu \quad (3.30)$$

The description of ψ_i is improved by increasing the number of basis functions used. If φ_μ are taken to be the atomic orbitals at the consistent atoms, (3.30) is called a linear combination of atomic orbitals (LCAO). The chosen basis functions should be easy to calculate and have the behavior, which agrees with the physics of the problem.

For small and highly symmetric systems, such as atoms and diatomic molecules, the Hartree-Fock equations may be solved numerically. This approach becomes impractical for large and lowly symmetric systems. Roothaan and Hall suggested the use of the unknown spatial basis functions in solving the complicated HF equation (3.29). The Roothaan-Hall equation is

$$\sum_{v=1}^n (F_{\mu v} - \epsilon_i S_{\mu v}) C_{v i} = 0 \quad , \quad \mu = 1, 2, \dots, n \quad (3.31)$$

integrating the Roothaan-Hall equation (for closed shell system) yields.

$$\sum_v C_{v i} \int dr_1 \varphi_\mu^*(1) f(1) \varphi_v(1) = \epsilon_i \sum_v C_{v i} \int dr_1 \varphi_\mu^*(1) \varphi_v(1) \quad (3.32)$$

$$\sum_v F_{\mu v} C_{v i} = \epsilon_i \sum_v S_{\mu v} C_{v i} \quad , \quad i = 1, 2, \dots, k \quad (3.33)$$

or

$$\mathbf{FC} = \mathbf{SC}\epsilon \quad (3.34)$$

\mathbf{F} refers to the Fock matrix, which is the matrix representation of the Fock operator with the set of basis function $\{\varphi_\mu\}$,

$$F_{\mu v} = \int dr_1 \varphi_\mu^*(1) f(1) \varphi_v(1) \quad (3.35).$$

\mathbf{S} refers to the overlap matrix, which contains the overlap elements between basis functions,

$$S_{\mu\nu} = \int d\mathbf{r}_1 \phi_{\mu}^*(1) \phi_{\nu}(1) \quad (3.36)$$

\mathbf{C} is a $k \times k$ matrix of the expansion coefficient $C_{\mu i}$

$$\mathbf{C} = \begin{pmatrix} C_{11} & C_{12} & \cdots & C_{1k} \\ C_{21} & C_{22} & \cdots & C_{2k} \\ \vdots & \vdots & \ddots & \vdots \\ C_{k1} & C_{k2} & \cdots & C_{kk} \end{pmatrix} \quad (3.37)$$

and ε is a diagonal matrix of the orbital energies ε_i

$$\varepsilon = \begin{pmatrix} \varepsilon_1 & & & 0 \\ & \varepsilon_2 & & \\ & & \ddots & \\ 0 & & & \varepsilon_k \end{pmatrix} \quad (3.38)$$

substitute the Fock operator into (3.35)

$$\begin{aligned} F_{\mu\nu} &= \int d\mathbf{r}_1 \phi_{\mu}^*(1) h(1) \phi_{\nu}(1) + \sum_a^{N/2} \int d\mathbf{r}_1 \phi_{\mu}^*(1) [2J_a(1) - K_a(1)] \phi_{\nu}(1) \\ &= H_{\mu\nu}^{\text{core}} + \sum_a^{N/2} 2(\mu\nu | aa) - (\mu a | a\nu) \end{aligned} \quad (3.39).$$

The first term is a core-Hamiltonian matrix, which is integrals involving the one-electron operator $h(1)$ and the second term is the two-electron part.

If the linear expansion of molecular orbitals is inserted into the two-electron term, then the Fock matrix is written as

$$\begin{aligned}
F_{\mu\nu} &= H_{\mu\nu}^{\text{core}} + \sum_a \sum_{\lambda\sigma}^{N/2} C_{\lambda a} C_{\sigma a}^* [2(\mu 2 | \sigma \lambda) - (\mu\mu | \sigma\nu)] \\
&= H_{\mu\nu}^{\text{core}} + \sum_{\lambda\sigma} P_{\lambda\sigma} [(\mu(| \sigma\lambda) - \frac{1}{2}(\mu\mu | \sigma\nu)] \\
&= H_{\mu\nu}^{\text{core}} + G_{\mu\nu}
\end{aligned} \tag{3.40}$$

where $G_{\mu\nu}$ is the two-electron part of the Fock matrix, which depends on the density matrix $P_{\lambda\sigma}$ and a set of two-electron integrals.

$$P_{\lambda\sigma} = 2 \sum_a^{N/2} C_{\lambda a} C_{\sigma a}^* \tag{3.41}$$

Since the Fock matrix depends on the density matrix or, equivalently, on the expansion coefficients, the Roothaan-Hall equation is nonlinear and must be solved iteratively. The Roothaan-Hall equation in (3.34) is not the standard eigenvalue equation. To solve this equation, one must first transform to the eigenvalue equation. This can be done by normalizing the overlap matrix.

If $\{\varphi'_\mu\}$ is the transformed set of $\{\varphi_\mu\}$ according to

$$\varphi'_\mu = \sum_\nu X_{\nu\mu} \varphi_\nu \tag{3.42}$$

where they form an orthonormal set,

$$\int d\mathbf{r} \varphi_\mu'^*(\mathbf{r}) \varphi_\nu'(\mathbf{r}) = \delta_{\mu\nu} \tag{3.43}$$

then $S'_{\mu\nu}$ (overlap matrix of the transformed set) is

$$\begin{aligned}
\int d\mathbf{r} \varphi_\mu'^*(\mathbf{r}) \varphi_\nu'(\mathbf{r}) &= \int d\mathbf{r} \left[\sum_\lambda X_{\lambda\mu}^* \varphi_\lambda^*(\mathbf{r}) \right] \left[\sum_\sigma X_{\sigma\nu} \varphi_\sigma(\mathbf{r}) \right] \\
&= \sum_\lambda \sum_\sigma X_{\lambda\mu}^* \int d\mathbf{r} \varphi_\lambda^*(\mathbf{r}) \varphi_\sigma(\mathbf{r}) X_{\sigma\nu} \\
&= \sum_\lambda \sum_\sigma X_{\lambda\mu}^* S_{\lambda\sigma} X_{\sigma\nu} = \delta_{\mu\nu}
\end{aligned} \tag{3.44}$$

or

$$\mathbf{X}^t \mathbf{S} \mathbf{X} = \mathbf{1} = \mathbf{S}' \quad (3.45)$$

where \mathbf{X} must be nonsingular and possess an inverse \mathbf{X}^{-1} .

Then

$$\mathbf{S} = \mathbf{X} \mathbf{S}' \mathbf{X}^{-1} = \mathbf{X} \mathbf{S}' \mathbf{X}^t \quad (3.46)$$

substituting eq. (3.46) into eq. (3.34), one obtains

$$\begin{aligned} \mathbf{F} \mathbf{C} &= \mathbf{X} \mathbf{S}' \mathbf{X}^t \mathbf{C} \boldsymbol{\varepsilon} \\ \mathbf{X}^{-1} \mathbf{F} \mathbf{X} (\mathbf{X}^{-1} \mathbf{C}) &= \mathbf{S}' (\mathbf{X}^{-1} \mathbf{C}) \boldsymbol{\varepsilon} \\ \mathbf{F}' \mathbf{C}' &= \mathbf{C}' \boldsymbol{\varepsilon} \end{aligned} \quad (3.47)$$

The Roothaan-Hall equation cannot be solved analytically. The illustration of SCF procedure²² for solving the Roothaan-Hall equation is given in Fig. 3.2.

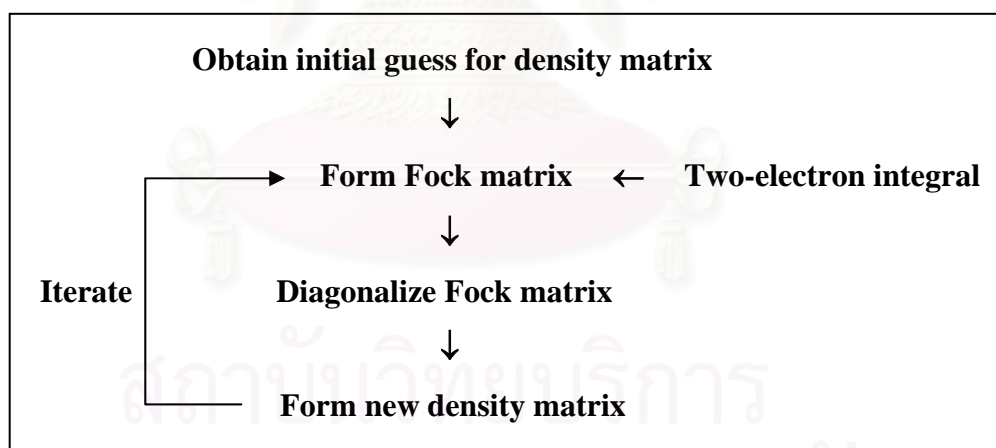


Fig. 3.2 Illustration of SCF procedure.

3.9 Basis Sets¹⁸⁻²¹

One of the approximations in solving the Schrödinger equation is the introduction of a basis set. An unknown molecular orbital (MO) are expanded in a set of known AO functions. A complete basis set contains an infinite number of functions, which is impossible in actual calculations. Finite atom-center basis sets are commonly used. Basis sets should be chosen as large as one is able to afford. However, for a basis set of M functions, about $M^4/8$ two-electron integrals $(\chi_a \chi_b | \chi_c \chi_d)$ are to be calculated and the type of basis functions used also influence the accuracy. Therefore, basis sets should be chosen as small as compatible with the required accuracy.

Slater and Gaussian Type Orbitals

There are two types of basis functions commonly used in electronic structure calculations; Slater Type Orbitals (STOs) and Gaussian Type Orbitals (GTOs).

Slater type orbitals have the functional form:

$$\chi_{\zeta,n,l,m}(r, \theta, \varphi) = N Y_{l,m}(\theta, \varphi) r^{n-1} e^{-\zeta r} \quad (3.48)$$

where $Y_{l,m}$ is the spherical harmonic functions,

$$Y_{l,m}(\theta, \varphi) = \Theta_{l,m}(\theta) \cdot \Phi_m(\varphi) = \sqrt{\frac{(2l+1)(l-|m|)!}{2(l+|m|)!}} P_l^{|m|}(\cos\theta) \cdot \frac{1}{\sqrt{2\pi}} \cdot e^{im\varphi} \quad (3.49),$$

N is normalization constant, n is the principal quantum number and ζ is exponent of the radial function. The exponential depend on the distance between the nucleus and the electron similar to the exact orbitals for the hydrogen atom. However, two electron integrals of polyatomic molecules are difficult to calculate when three and four atomic centers a, b, c, d are involved. Consequently, STOs are suitable for atomic, diatomic systems and in semi-empirical methods where all three-and four-center integrals are neglected.

Gaussian type orbitals (GTOs) can be written in terms of spherical or Cartesian coordinates:

$$\chi_{\zeta,n,l,m}(r, \theta, \varphi) = NY_{l,m}(\theta, \varphi)r^{(2n-2-l)}e^{-\zeta r^2} \quad (3.50)$$

$$\chi_{\zeta,l_x,l_y,l_z}(x, y, z) = Nx^{l_x}y^{l_y}z^{l_z}e^{-\zeta r^2} \quad (3.51)$$

where the type of orbital can be determined by the angular momentum ($l = l_x + l_y + l_z$). The spherical GTOs can be formed by linear combination of cartesian GTOs of the same l value. For $l > 1$, the number of spherical and cartesian GTOs differ, i.e. d-type GTOs ($l = 2$) have five spherical GTOs, but there appear to be six cartesian GTOs ($x^2, y^2, z^2, xy, xz, yz$), which may be transformed to the five spherical d-functions and one additional s-function ($x^2 + y^2 + z^2$). Similarly, f-type GTOs, ten cartesian GTOs may be transformed to the seven spherical f-functions and one set of spherical p-functions. The use of only the spherical components reduces the problems of linear dependence for large basis sets.

However, GTOs exhibit the wrong behavior near the nucleus ($r \approx 0$), the cusp, and for $r \rightarrow \infty$, where the radial function is vanished too fast (Fig 3.3). Therefore, many more GTOs are required to achieve the same accuracy as with STOs. Because the faster calculation with four-center two-electron integrals GTOs are the most common basis functions used nowadays.

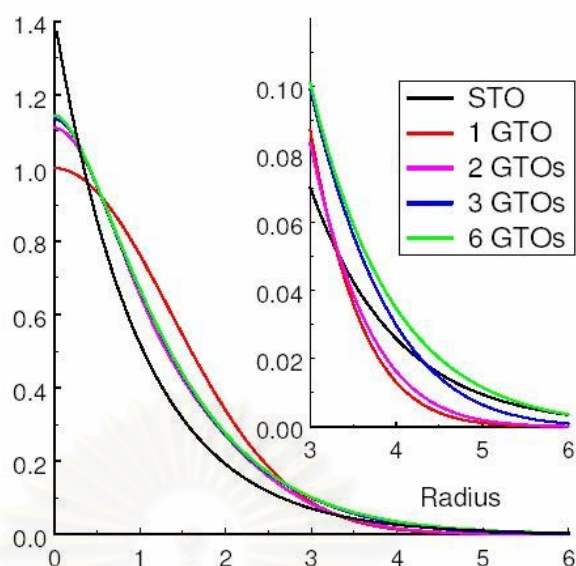


Fig. 3.3 The approximation of STO by a set of several GTOs.

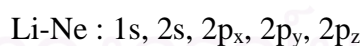
3.9.1 Minimal Basis Set

The minimal basis sets is the representation of a Slater type orbitals with n Gaussian functions (STO- n G), which only enough functions are employed to contain all the electrons of the neutral atoms, one function per atomic orbital, *i.e.*

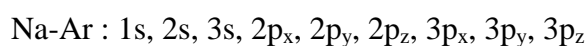
hydrogen and helium are represent by a single s-function (1-AO):



the first row in the periodic table are represent by two s-functions and one set of p-functions (5-AOs):



and the second row in the periodic table are represent by three s-functions and two sets of p-functions (9-AOs):



The minimal basis sets are well known to accompany with several deficiencies. The atoms at the end of the period that have more number of electrons are described using

the same number of basis functions as the atoms at the beginning of the period. Furthermore, the radial exponents are not allowed to vary during the calculation. Consequently, the orbital cannot contract in size in accordance with the nature of molecules.

3.9.2 Extended Basis Set

To improve the minimal basis sets, the number of all basis functions must be increased. These basis functions are the linear combination of the contracted and diffuse functionals. The size of orbital can be modified during the course of calculation.

The double zeta (DZ) basis is described by double of all STOs minimal basis functions:

H-He : 1s and 1s'

Li-Ne : 1s and 1s', 2s and 2s', 2p_x, 2p_y, 2p_z and 2p_x', 2p_y', 2p_z'

Na-Ar : 1s and 1s', 2s and 2s', 3s and 3s', 2p_x, 2p_y, 2p_z and 2p_x', 2p_y', 2p_z',
3p_x, 3p_y, 3p_z and 3p_x', 3p_y', 3p_z'

Similarly, the triple zeta (TZ) basis is described by triple of all STOs minimal basis functions:

H-He : 1s, 1s' and 1s''

Li-Ne : 1s, 1s' and 1s'', 2s, 2s' and 2s'',
2p_x, 2p_y, 2p_z, 2p_x', 2p_y', 2p_z' and 2p_x'', 2p_y'', 2p_z''

Na-Ar : 1s, 1s' and 1s'', 2s, 2s' and 2s'', 3s, 3s' and 3s'', 2p_x, 2p_y, 2p_z,
2p_x', 2p_y', 2p_z' and 2p_x'', 2p_y'', 2p_z'', 2p_x'', 2p_y'', 2p_z'',
and 2p_x'', 2p_y'', 2p_z''

Double and triple zeta basis yields a better description of the charge distribution compare to minimal basis. Example of the charge distribution of HCN is given in Fig. 3.4.

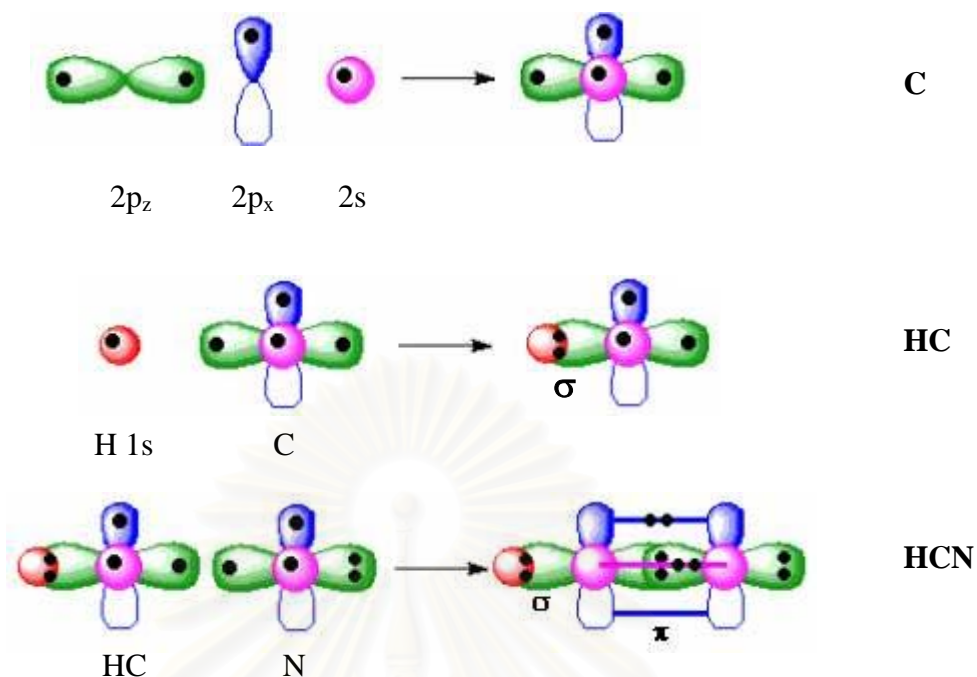


Fig. 3.4 Charge distribution of HCN molecule.

Double and triple zeta basis has the flexibility to describe the charge distribution in both to HCN molecule; C-H σ -bond consists of the H 1s orbital and the C $2P_z$, C-N π -bond is made up of C and N $2P_x$ and $2P_y$ AOs. The optimal AO coefficient (in MO expansion) of the tighter inner P_z function on C will be larger in the C-H bond. Whereas the more diffuse outer P_x and P_y function will have larger AO coefficient in the π -bond. An alternative to the double zeta basis approach is to double the number of functions used to describe the valence electrons but to keep a single function for the inner shells called “split valence double zeta basis”.

For example, carbon 6-31G

1s : 1 STO of 6 GTOs

2s/2p : 1 STO of 3 GTOs for contracted part plus 1 additional GTO for diffuse part

Examples of other valence double zeta basis sets such as 3-21G, Dunning’s DZV, etc. Furthermore, there are still “split valence triple zeta basis” such as 6-311G, Dunning basis TZV, etc.

3.9.3 Polarization Basis Set

The most common used polarization function comes from the Pople group. The polarization functions describe atomic orbital distortions due to bonding. In molecular system, it is clear that the influence of the other nucleus will distort or polarize the electron density near the nucleus, consequently, the orbitals have more flexible shapes than the orbital shapes in the free atoms. This is best accomplished by adding in basis functions of higher angular momentum quantum number. Thus, the spherical s-orbital can be distorted by mixing in orbital of p symmetry. The electron distribution along the bond will be different that perpendicular to the bond. The positive lobe at one side increases the value of the orbital while the negative lobe at the other side decreases the orbital. Similarly, the p-orbitals can be polarized by mixing in an orbital of d symmetry. For example, Fig. 3.5 shows a polarization of 1s-orbital is induced by $2p_z$ -function for H atom in HCN.

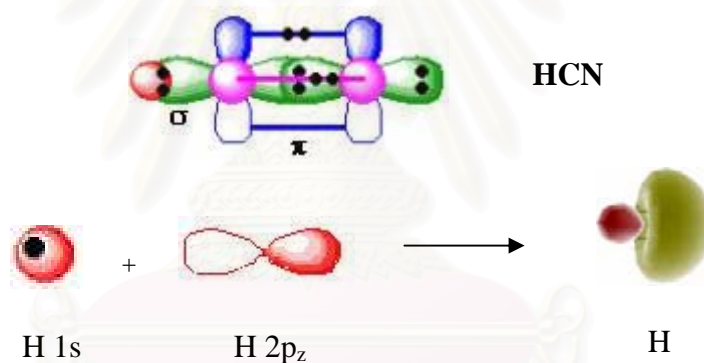


Fig. 3.5 $2p_z$ -function induces a polarization of 1s-orbital for H atom in HCN.

The obtained results from adding polarization functions to these split valence basis sets are a significant improvement, particularly for accurately determination of bond angles. Examples of these basis sets are 6-31G(d), 6-31G(d, p), etc.

3.9.4 Diffuse Basis Set

In some cases, the normal basis functions are not adequate for calculation of dipole moment, polarizability, particularly, in excited states and in anions where the electron density is spread out all over the molecule. Thus, the orbitals can be more spread out by adding diffuse functions as single GTOs, not contracting them together. Examples of these basis sets are 6-31G+, 6-31G++(d, p) and 6-311G++, etc.

3.10 Density Functional Theory (DFT)²³

Density functional theory (DFT) is the theory, which describe nature of electron base on the electron density distribution $\rho(\mathbf{r})$ instead of the many-electron wavefunction $\Psi(\mathbf{r}, r_2, r_3, \dots)$. The electron density distribution $\rho(\mathbf{r})$ is the square of the wave function, integrated over N-1 electron coordinates, this only depends on three coordinates, independently of the system size.

$$\rho(\bar{\mathbf{r}}) = N \cdot \int \dots \int |\Psi(\bar{x}_1, \bar{x}_2, \dots, \bar{x}_N)|^2 ds_1 d\bar{x}_2 \dots d\bar{x}_N \quad (3.52)$$

where

$$\begin{aligned} \rho(\bar{\mathbf{r}} \rightarrow \infty) &= 0 \\ \int \rho(\bar{\mathbf{r}}) d\bar{\mathbf{r}} &= N \end{aligned} \quad (3.53)$$

Since, the probability of finding any of the N electrons within the volume element $d\bar{\mathbf{r}}$ (with arbitrary spin) is determined.

DFT can be used to calculate all properties of molecules, clusters and solids, for examples, the ground state density $\rho(\mathbf{r})$, the full N-particle ground state wave function $\Psi(\mathbf{r}_1, \dots, \mathbf{r}_N)$, the electrical polarizability, vibrational force constant, energy, and potential energy surfaces for chemical reactions, etc. The goal of DFT method is to design functionals connecting the electron density with the energy.

Thomas-fermi proposed one of the earliest tractable schemes for solving the many-electron problem.²⁴ They state that the electron density $\rho(\mathbf{r})$ is the central variable rather than the wavefunction, and the total energy of a system is written as a functional $E^{\text{TF}}[\rho(\mathbf{r})]$. The thomas-Fermi energy functional is composed of three terms.

$$E^{\text{TF}}[\rho(\mathbf{r})] = A_k \int \rho(\mathbf{r}_i)^{5/3} d\mathbf{r}_i + \int \rho(\mathbf{r}_i) v_{\text{ext}}(\mathbf{r}_i) d\mathbf{r}_i + \frac{1}{2} \iint \frac{\rho(\mathbf{r}_i)\rho(\mathbf{r}_j)}{|\mathbf{r}_i - \mathbf{r}_j|} d\mathbf{r}_i d\mathbf{r}_j \quad (3.54)$$

where the first term is the electronic kinetic energy associated with a system of non-interacting electron in a homogeneous electron gas, which $A_k = \frac{3}{10} (3\pi^2)^{2/3}$, the second term is the classical electrostatic kinetic energy association between the nuclei and the electrons, which $v_{\text{ext}}(\mathbf{r})$ is the static Coulomb potential arising from the nuclei,

$$v_{\text{ext}}(\mathbf{r}) = -\sum_{A=1}^N \frac{Z_A}{|\mathbf{r} - \mathbf{R}_A|} \quad (3.55),$$

and the third term represents electron-electron repulsion, known as the Hartree energy.

To obtain the groundstate density and energy of a system, (3.51) must be minimised subject to the constraint that the number of electrons is conserved, which can be performed using the technique of Lagrange multipliers. In general terms, the minimization of a functional, subject to the constraint, leads to the following stationary condition. Minimizing lead to the solution of the Thomas-Fermi equation,

$$\delta \left\{ E^{\text{TF}}[\rho(\mathbf{r})] - \mu \left(\int \rho(\mathbf{r}) d\mathbf{r} - N \right) \right\} = 0 \quad (3.56)$$

Thus, the so-called Thomas-Fermi equations can be written as

$$\frac{3}{5} A_k \rho(\mathbf{r}_i)^{2/3} + v_{\text{ext}}(\mathbf{r}_i) + \int \frac{\rho(\mathbf{r}_j)}{|\mathbf{r}_i - \mathbf{r}_j|} d\mathbf{r}_j - \mu = 0 \quad (3.57)$$

where μ is Lagrange multipliers constant

However, Thomas-Fermi theory suffers from many deficiencies, probably the most serious defect is that it does not predict bonding between atoms so molecules and solids cannot form in this theory. The main source of error comes from approximating the kinetic energy in such a crude way. The kinetic energy represents a substantial portion of the total energy of a system and so even small errors prove disastrous. Another shortcoming is the over-simplified description of the electron-electron interactions, which are treated classically and so do not take account of quantum phenomenon such as the exchange interaction.

Dirac²⁴ developed an approximation for the exchange interaction based on the homogeneous electron gas.²⁴ The formula is a local functional of the density,

$$E_x[\rho(\mathbf{r})] = -\frac{3}{4} \left(\frac{3}{\pi} \right)^{1/3} \int \rho(\mathbf{r})^{4/3} d\mathbf{r} \quad (3.58)$$

(3.58) is usually written in terms of the exchange energy density,

$$E_{xc}[\rho(\mathbf{r})] = \int \rho(\mathbf{r}) \varepsilon_{xc}[\rho(\mathbf{r})] d\mathbf{r} \quad (3.59)$$

where $\varepsilon_{xc}[\rho(\mathbf{r})]$ can be given simply in terms of the seitz radius r_s ,

$$\varepsilon_{xc}[\rho(\mathbf{r})] = -\frac{3}{4} \left(\frac{9}{4\pi^2} \right)^{1/3} \frac{1}{r_s} \approx -\frac{0.4582}{r_s} \quad (3.60)$$

The Dirac exchange term was incorporated into Thomas-Fermi theory. However, the inclusion of local exchange did not improve the Thomas-Fermi method.

Hohenberg and Kohn²⁵ proved that an exact theory could be based on the density. They formally established the $\rho(\mathbf{r})$ as the central describing electron interactions, so devised the formally exact groundstate method known as density functional theory (DFT). The Hohenberg-Kohn theorems relate to any system consisting of electrons moving under the influence of an external potential, $v_{\text{ext}}(\vec{r})$, which the two Hohenberg-Kohn theorems are now described.

The first Hohenberg-Kohn theorem

The external potential, $V_{\text{ext}}(\vec{r})$, and hence the total energy, is a unique functional of the electron density $\rho(\mathbf{r})$,

$$v_{\text{ext}}(\vec{r}) \Rightarrow \rho(\vec{r}) \quad (3.61).$$

The energy functional $E[\rho(\mathbf{r})]$ can be written in terms of the external potential in the following way,

$$E[\rho(\mathbf{r})] = \int \rho(\mathbf{r}) v_{\text{ext}}(\mathbf{r}) d\mathbf{r} + F[\rho(\mathbf{r})] \quad (3.62)$$

Where $F[\rho(\mathbf{r})]$ is an unknown, but otherwise universal functional of the electron density only.

Minimizes the expectation value gives the ground state energy,

$$E[\rho(r)] = \langle \Psi | \hat{H} | \Psi \rangle \quad (3.63)$$

Hamiltonian for the system can be written as

$$\hat{H} = \hat{F} + \hat{V} \quad (3.64)$$

where F is the electronic Hamiltonian

To prove the first theorem, there are two different external potentials $v_{\text{ext}}(r)$, and $v'_{\text{ext}}(r)$, that give rise to the same density $\rho(r)$. The associated Hamiltonians, H and H' , will have different groundstate wavefunctions, Ψ , and Ψ' that each yields $\rho(r)$.

$$H = H_0 + v_{\text{ext}}(r) \quad ; \quad H\Psi = E\Psi \quad (3.65)$$

$$H' = H_0 + v'_{\text{ext}}(r) \quad ; \quad H'\Psi' = E'\Psi' \quad (3.66)$$

Using the variational principle one can write the inequality,

$$\begin{aligned} E_0 < \langle \Psi' | H | \Psi' \rangle &= \langle \Psi' | H' | \Psi' \rangle + \langle \Psi' | H - H' | \Psi' \rangle \\ &= E'_0 + \int \rho(r) [v_{\text{ext}}(r) - v'_{\text{ext}}(r)] dr \end{aligned} \quad (3.67)$$

It is at this point that the Hohenberg-Kohn theorems apply rigorously to the groundstate only. Adding the interchanged inequality to (3.63) leads to the result,

$$E_0 + E'_0 < E'_0 + E_0 \quad (3.68)$$

It is concluded that there cannot be two different external potentials $v_{\text{ext}}(r)$ and $v'_{\text{ext}}(r)$ that give the same density $\rho(r)$ for their ground states. Since the complete ground state energy E_0 is a unique functional of the density $\rho(r)$, so must be its individual parts. One can write.

The second Hohenberg-Kohn theorem

The groundstate energy can be obtained variationally, the trial density that minimizes the total energy is the exact groundstate density,

To prove the second theorem; $\rho(r)$ determines $v_{\text{ext}}(r)$; N and $v_{\text{ext}}(r)$ determine H and Ψ . Thus, Ψ is a functional of $\rho(r)$ and the expectation value of F is also a functional of $\rho(r)$,

$$F[\rho(r)] = \langle \Psi | F | \Psi \rangle \quad (3.69)$$

If a density that is the ground-state of some external potential is known as v -representable, the v -representable energy functional can be defined in which the external potential is unrelated to another density $\rho'(r)$,

$$E_v[\rho(r)] = \int \rho'(r) v_{\text{ext}}(r) dr + F[\rho'(r)] \quad (3.70)$$

Using the variational principle,

$$\langle \Psi' | \hat{F} | \Psi' \rangle + \langle \Psi' | \hat{v}_{\text{ext}} | \Psi' \rangle > \langle \Psi | \hat{F} | \Psi \rangle + \langle \Psi | \hat{v}_{\text{ext}} | \Psi \rangle \quad (3.71)$$

This lead to,

$$\int \rho'(r) v_{\text{ext}}(r) dr + F[\rho'(r)] > \int \rho(r) v_{\text{ext}}(r) dr + F[\rho(r)] \quad (3.72)$$

Thus, the second Hohenberg-Kohn theorem is obtained

$$E_v[\rho'(r)] = E_v[\rho(r)] \quad (3.73)$$

Although the Hohenberg-Kohn theorems are extremely powerful, they do not offer a way of computing the groundstate density of a system in practice.

Kohn and Sham²⁶ introduced the use of orbital for the Hohenberg-Kohn theorem.

For N-noninteracting system (no e-e repulsion), the Hamiltonian is given as

$$\begin{aligned} H_s &= \sum_i^N h_s(\mathbf{i}) + v_s(\mathbf{r}) \\ &= \sum_i^N \left[-\frac{1}{2} \nabla_i^2 \right] + v_s(\mathbf{r}) \end{aligned} \quad (3.74)$$

The non-interacting wavefunction Ψ_s is

$$\Psi_s = \frac{1}{\sqrt{N!}} |\Psi_1 \Psi_2 \dots \Psi_N\rangle \quad (3.75).$$

Since

$$\begin{aligned} E_0[\rho] &= \langle \Psi_s | \sum_i^N -\frac{1}{2} \nabla_i^2 + v_s(\mathbf{r}) | \Psi_s \rangle \\ &= T_s[\rho] + V_{Ne}[\rho] \end{aligned} \quad (3.76)$$

and

$$\begin{aligned} T_s[\rho] &= \sum_i^N \langle \Psi_i | -\frac{1}{2} \nabla_i^2 | \Psi_i \rangle \\ &= F_{HK}[\rho] \end{aligned} \quad (3.77),$$

then for the N-interacting system (3.67) can be modified as

$$F_{HK}[\rho] = T_s[\rho] + J[\rho] + E_{xc}[\rho] \quad (3.78)$$

where the last term, $E_{xc}[\rho]$, is the exchange correlation functional which is

$$E_{xc}[\rho] = T[\rho] - T_s[\rho] + V_{ee}[\rho] - J[\rho] \quad (3.79)$$

and $J[\rho]$, the coulomb interaction, is

$$J[\rho] = \int \frac{\rho_1(\vec{r}_1) \rho_2(\vec{r}_2)}{r_{12}} d\vec{r}_1 d\vec{r}_2 \quad (3.80)$$

The density can also be written in terms of orbital as

$$\rho(\mathbf{r}) = \sum_i^N |\Psi_i(\mathbf{r})|^2 \quad (3.81)$$

Similar to Hartree-Fock theory, the variational principle is applied, which lead finally to the self-consistent Kohn-Sham equations.

$$\hat{f}^{\text{KS}} \phi_i = \varepsilon_i \phi_i \quad (3.82)$$

with the Kohn-Sham operator

$$\hat{f}^{\text{KS}} = -\frac{1}{2} + \int \frac{\rho(\mathbf{r}_j)}{r_{ij}} d\mathbf{r}_j + v_{\text{xc}}[\rho] + \sum_A \frac{Z_A}{r_{iA}} \quad (3.83)$$

The major problem in DFT is deriving suitable formulas for the exchange-correlation term. Using the same algorithms as in Hartree-Fock theory, including the usage of basis functions and the self-consistent field (SCF) approach, can solve The Kohn-Sham equation. However, the Kohn-Sham orbitals (ϕ_i) are not the same as the Hartree-Fock orbitals (ϕ_i^{HF}), which implies that they also lack the physical interpretation of the Hartree-Fock one electron molecular orbitals.

3.10.1 The Local Density Approximation

The Local Density approximation (LDA)^{27, 28} assumes that the density locally can be treated as a uniform electron gas. The density is a slowly varying function. The exchange correlation energy is given as

$$E_{\text{xc}}[\rho] = E_{\text{x}}[\rho] + E_{\text{c}}[\rho] \quad (3.84)$$

where $E_{\text{x}}[\rho]$ is accounting for the pure exchange, and $E_{\text{c}}[\rho]$ is the correlation part.

Local Spin Density Approximation is used to replace LDA where the spin densities are not the same,

$$E_x[\rho] = E_x^\alpha[\rho_\alpha] + E_x^\beta[\rho_\beta] \quad (3.85)$$

$$E_c[\rho] = E_c^{\alpha\alpha}[\rho_\alpha] + E_c^{\beta\beta}[\rho_\beta] + E_c^{\alpha\beta}[\rho_\alpha, \rho_\beta] \quad (3.86)$$

This may also be written in terms of the spin polarization, ζ

$$\zeta = \frac{\rho^\alpha - \rho^\beta}{\rho^\alpha + \rho^\beta}, \frac{4}{3}\pi r_s^3 = \rho^{-1} \quad (3.87)$$

For closed-shell systems LSDA is equal to LDA due to the density α and β are the same. LSDA is often used interchangeably with LDA.

To include the correlation term, which is determined by Monte Carlo method. Vosko, Wilk and Nusair (VWN) constructed the interpolation formula to use the obtain result in DFT calculation. The functional can be written as

$$\varepsilon_c^{\text{VWN}}(r_s, \zeta) = \varepsilon_c(r_s, 0) + \varepsilon_a(r_s) \left[\frac{f(\zeta)}{f''(\zeta)} \right] [1 - \zeta^4] + [\varepsilon_c(r_s, 1) - (\varepsilon_c(r_s, 0))] f(\zeta) \zeta^4 \quad (3.88)$$

$$f(\zeta) = \frac{(1 + \zeta)^{4/3} + (1 - \zeta)^{4/3} - 2}{2(2^{1/3} - 1)} \quad (3.89)$$

The $\varepsilon_c(r_s, \zeta)$ and $\varepsilon_a(r_s)$ functionals are parameterized as

$$\varepsilon_{c/a}(x) = A \left\{ \ln \frac{x^2}{X(x)} + \frac{2b}{Q} \tan^{-1} \left(\frac{Q}{2x + b} \right) - \frac{bx_0}{X(x_0)} \left[\ln \frac{(x - x_0)^2}{X(x)} + \frac{2(b + 2x_0)}{2} \tan^{-1} \left(\frac{Q}{2x + b} \right) \right] \right\} \quad (3.90)$$

where

$$x = \sqrt{r_s}$$

$$X(x) = x^2 + bx + c$$

$$Q = \sqrt{4c - b^2}$$

The parameters A, x_0 , b and c are fitting constants, different for $\varepsilon_c(r_s, 0)$, $\varepsilon_c(r_s, 1)$ and $\varepsilon_a(r_s)$.

Perdew and Wang give a modified form for $\varepsilon_{c/a}(\mathbf{r}_s)$ obtain the PW91 functional,

$$\varepsilon_{c/a}^{\text{PW91}} = -2a\rho(1 + \alpha x^2) \ln\left(1 + \frac{1}{2\alpha(\beta_1 x + \beta_2 x^2 + \beta_3 x^3 + \beta_4 x^4)}\right) \quad (3.91)$$

where a , α , β_1 , β_2 , β_3 and β_4 are suitable constants.

The LSDA approximation underestimates the exchange energy by ~10%, whereas the electron correlation and bond strengths is overestimated. However, LSDA methods are often found to provide results with accuracy similar to that obtained by Hartree-Fock method.

3.10.2 The Generalized Gradient Approximation

Generalized Gradient Approximation (GGA) methods²⁹⁻³³ are the improvement of LSDA with considering a non-uniform electron gas. The exchange and correlation energies depend not only on the electron density, but also on derivatives of the density.

In 1986, Perdew and Wang (PW86)²⁹ proposed modifying the LSDA exchange expression,

$$\varepsilon_x^{\text{PW86}} = \varepsilon_x^{\text{LDA}} \left(1 + ax^2 + bx^4 + cx^6\right)^{1/15} \quad (3.92)$$

$$x = \frac{|\nabla \rho|}{\rho^{4/3}}$$

where x is a dimensionless gradient variable, and a , b and c are suitable constants.

In 1988, Becke (B88)³⁰ modified the LSDA exchange energy, which can be given as

$$\begin{aligned} \varepsilon_x^{\text{B88}} &= \varepsilon_x^{\text{LDA}} + \Delta\varepsilon_x^{\text{B88}} \\ \Delta\varepsilon_x^{\text{B88}} &= -\beta\rho^{1/3} \frac{x^2}{1 + 6\beta \sinh^{-1} x} \end{aligned} \quad (3.93)$$

where β is parameter that is determined by fitting to known atomic data.

Perdew and Wang (PW91) have proposed an exchange functional similar to B88,

$$\varepsilon_x^{\text{PW91}} = \varepsilon_x^{\text{LDA}} \left(\frac{1 + xa_1 \sinh^{-1}(xa_2) + (a_3 + a_4 e^{-bx^2})x^2}{1 + xa_1 \sinh^{-1}(xa_2) + a_5 x^2} \right) \quad (3.94)$$

where a_1 - a_5 and b are suitable constants and $x = \frac{|\nabla \rho|}{\rho^{4/3}}$.

Lee, Yang and Parr (LYP)³¹ proposed the correlation energy. The functional can be given as

$$\varepsilon_c^{\text{LYP}} = -a \frac{\gamma}{(1+d\rho^{-1/3})} - ab \frac{\gamma e^{-c\rho^{-1/3}}}{9(1+d\rho^{-1/3})\rho^{8/3}} \left[18(2^{2/3})C_F(\rho_\alpha^{8/3} + \rho_\beta^{8/3}) - 18\rho t_w + \rho_\alpha(2t_w^\alpha + \nabla^2 \rho_\alpha) + \rho_\beta(2t_w^\beta + \nabla^2 \rho_\beta) \right] \quad (3.95)$$

$$t_w^\sigma = \frac{1}{8} \left(\frac{|\nabla \rho_\sigma|^2}{\rho_\sigma} \right) - \nabla^2 \rho_\sigma$$

$$\gamma = 2 \left[1 - \frac{\rho_\alpha^2 + \rho_\beta^2}{\rho^2} \right]$$

where the a , b , c and d parameters are determined by fitting to data for the helium atom. The t_w^σ functional is the local Weizsacker kinetic energy density and the γ - factor becomes zero when all the spins are aligned ($\rho = \rho_\alpha, \rho_\beta = 0$).

In 1991, Perdew and Wang proposed and modified a gradient correction to the LSDA result that can be written as

$$\varepsilon_c^{\text{PW91}} = \varepsilon_c^{\text{LDA}} + \Delta\varepsilon_c^{\text{PW91}}$$

$$\Delta\varepsilon_c^{\text{PW91}}[\rho] = \rho(H_0(t, r_s, \zeta) + H_1(t, r_s, \zeta)) \quad (3.96)$$

$$H_0(t, r_s, \zeta) = b^{-1} f(\zeta)^3 \ln \left[1 + a \frac{t^2 + At^4}{1 + At^2 + A^2 t^4} \right]$$

$$H_1(t, r_s, \zeta) = \left(\frac{16}{\pi}\right) (3\pi^2)^{1/3} [C(\rho) - c] f(\zeta)^3 t^2 e^{-dx^2/f(\zeta)^2}$$

$$f(\zeta) = \frac{1}{2} \left((1+\zeta)^{2/3} + (1-\zeta)^{2/3} \right)$$

$$C(\rho) = \ell_1 + \frac{\ell_2 + \ell_3 r_s + \ell_4 r_s^2}{1 + \ell_5 r_s + \ell_6 r_s^2 + \ell_7 r_s^3}$$

$$t = \left(\frac{192}{\pi^2}\right)^{1/6} \frac{|\nabla\rho|}{2f(\zeta)\rho^{7/6}}$$

$$A = a \left[e^{-b\varepsilon_c(r_s, \zeta)/f(\zeta)^3} - 1 \right]^{-1}$$

where a , b , c and d are suitable constants and $\ell_1 - \ell_7$ are numerical constants.

The several proposed functionals have restricted to predict correlation energies for one-electron systems and failed to have the exchange energy cancel the Coulomb self-repulsion. In 1995, Becke proposed the functionals which does not have these problems,

$$\varepsilon_c^{B95} = \varepsilon_c^{\alpha\beta} + \varepsilon_c^{\alpha\alpha} + \varepsilon_c^{\beta\beta}$$

$$\varepsilon_c^{\alpha\beta} = \left[1 + a(x_\alpha^2 + x_\beta^2) \right]^{-1} \varepsilon_c^{PW91, \alpha\beta}$$

$$\varepsilon_c^{\sigma\sigma} = \left[1 + bx_\sigma^2 \right]^{-2} \frac{D_\sigma}{D_\sigma^{LDA}} \varepsilon_c^{PW91, \sigma\sigma} \quad (3.97)$$

$$D_\sigma = \sum_i^N |\nabla\phi_i|^2 - \frac{(\nabla\rho_\sigma)^2}{4\rho_\sigma}$$

$$D_\sigma^{LDA} = 2^{5/3} C_F \rho_\sigma^{5/3}$$

$$x = \frac{|\nabla\rho|}{\rho^{4/3}}$$

where σ is α or β spins, a and b are fitting parameters and ε_c^{PW91} is the Perdew-Wang parameterization of the LSDA correlation functional.

Becke proposed the Becke-3 functional for E_{xc} which included three semi-empirical parameters, a_0 , a_x , and a_c

$$E_{xc} = E_{xc}^{HF} + (1 - a_0)E_x^{LDA} + a_x \Delta E_x^B + (1 - a_c)E_c^{VWN} \quad (3.98)$$

3.10.3 Hybrid Functional

Hybrids are an interesting class of functionals, which combine exact Hartree-Fock exchange with conventional GGAs. The general form is

$$E_{XC}^{hybrid} = \alpha(E_x^{HF} - E_x^{GGA}) + E_{xc}^{GGA} \quad (3.99)$$

Hybrids give significant improvement over GGAs for many molecular properties. Possibly the most widely used hybrid is the B3LYP functional, which the Becke-3 functional is combined with the Lee-Yang-Parr (LYP) correlation functional,

$$E_{xc} = E_{xc}^{HF} + (1 - a_0)E_x^{LDA} + a_x \Delta E_x^B + (1 - a_c)E_c^{VWN} + a_c \Delta E_c^{LYP} \quad (3.100)$$

CHAPTER 4

CALCULATIONS

Molecular Dynamic (MD) simulation and quantum calculation were employed throughout the work. The MD simulations were applied to obtain ZSM-5 structures. The quantum chemical calculations were applied to gain exchange energies and structures of CuZSM-5.

4.1 Molecular Dynamic (MD) Simulation

4.1.1 Preparation of ZSM-5 Structure

MD simulations were performed on model of silicalite-1 (MFI) in which 2 Si atoms in the unit cell were replaced by 2 Al atoms at 2 tetrahedral (T) sites (Si/Al=47) and negative charges of the Al-substituted T-site were compensated by H⁺. There are 23 possible substitutions of this kind¹¹ as given in Table 4.1.

Table 4.1 All possible substitutions for 2 Al in MFI.

Possible substitution of Al sites	Possible substitution of Al sites
T1T1	T6T6
T1T6	T6T12
T1T7	T7T9-model1
T2T2	T7T9-model2
T2T5	T7T12-model1
T3T3	T7T12-model2
T3T9	T7T12-model3
T4T4-model1	T8T8
T4T4-model2	T9T10
T4T10	T9T12
T5T5	T11T11
T5T12	

However, only 4 possible substitutions, *i.e.*, T6T12, T8T8, T7T12-model1, and T7T12-model2 were selected. These substitutions from now called “exchanged sites”. The sites situate in the cavity of the straight channel and T12 is at the intersection between the straight and sinusoidal channels. Furthermore, previous MD study of Cu^{2+} exchange on double exchanged CuZSM-5¹¹ showed that favorable exchanges are site for 5-T ring T6T12 and site for 6-T ring T7T12.

To obtain structure for ZSM-5 or HZSM-5, MD simulations were performed. The MD simulations were carried out for all HZSM-5 structures studied using CVFF force field, and NVT ensemble. All structures used runtime of at least 2000 ps, and time step 0.1 fs at 300 K. Structures of HZSM-5 at 4 adsorbed sites were given in Figs. 4.1a-d.

The MD simulations were not performed in this work but the structures were taken from works of Mr.Ukrid Poombub.³⁵

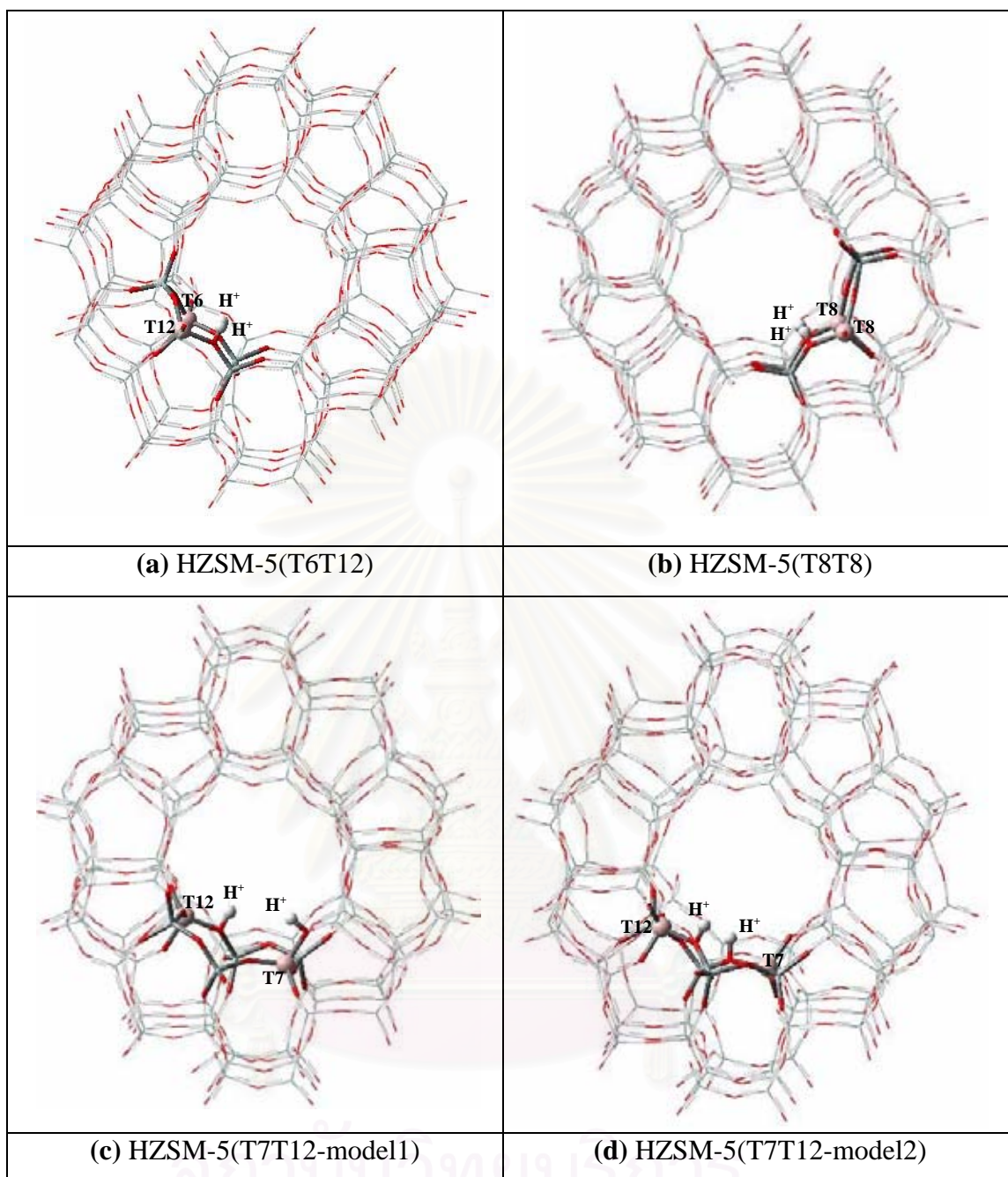


Fig. 4.1 Simulated HZSM-5 structure for Al-substitution at 4 exchanged sites: (a) HZSM-5(T6T12), (b) HZSM-5(T8T8), (c) HZSM-5(T7T12-model1), and (d) HZSM-5(T7T12-model2).

4.2 Quantum Calculation

4.2.1 HZSM-5 Cluster Model

Partial geometry optimization using B3LYP method with 6-31G(d,p) basis set were performed on cluster models that were obtained from the MD simulations. According to exchanged sites, two types of cluster models can be obtained. One is 5-T ring; HZSM-5(T6T12) exchanged site. And others are 6-T ring; HZSM-5(T8T8), HZSM-5(T7T12-model1), HZSM-5(T7T12-model2) exchanged site. For each obtained cluster model, all O atoms at the edge of ring (T-O-Si) were terminated and saturated with H atoms in replacement of Si atoms. Thus, H⁺T6-H⁺T12 exchanged site, H⁺₂[Al₂Si₃O₁₅H₁₀], includes 32 atoms and H⁺T8-H⁺T8, H⁺T7-H⁺T12(model1), and H⁺T7-H⁺T12(model2) exchanged site, H⁺₂[Al₂Si₄O₁₈H₁₂], consist of 38 atoms each. Geometrical parameters of the cluster were fixed except H⁺, O-H bond lengths, and T-O-H bond angles (\angle T-O-H) were optimized by setting one parameter for all O-H and one for \angle T-O-H. All calculations were performed at room temperature using the Gaussian 98 program.³⁴ The structures of the 4 models were shown in Figs. 4.2a-d.

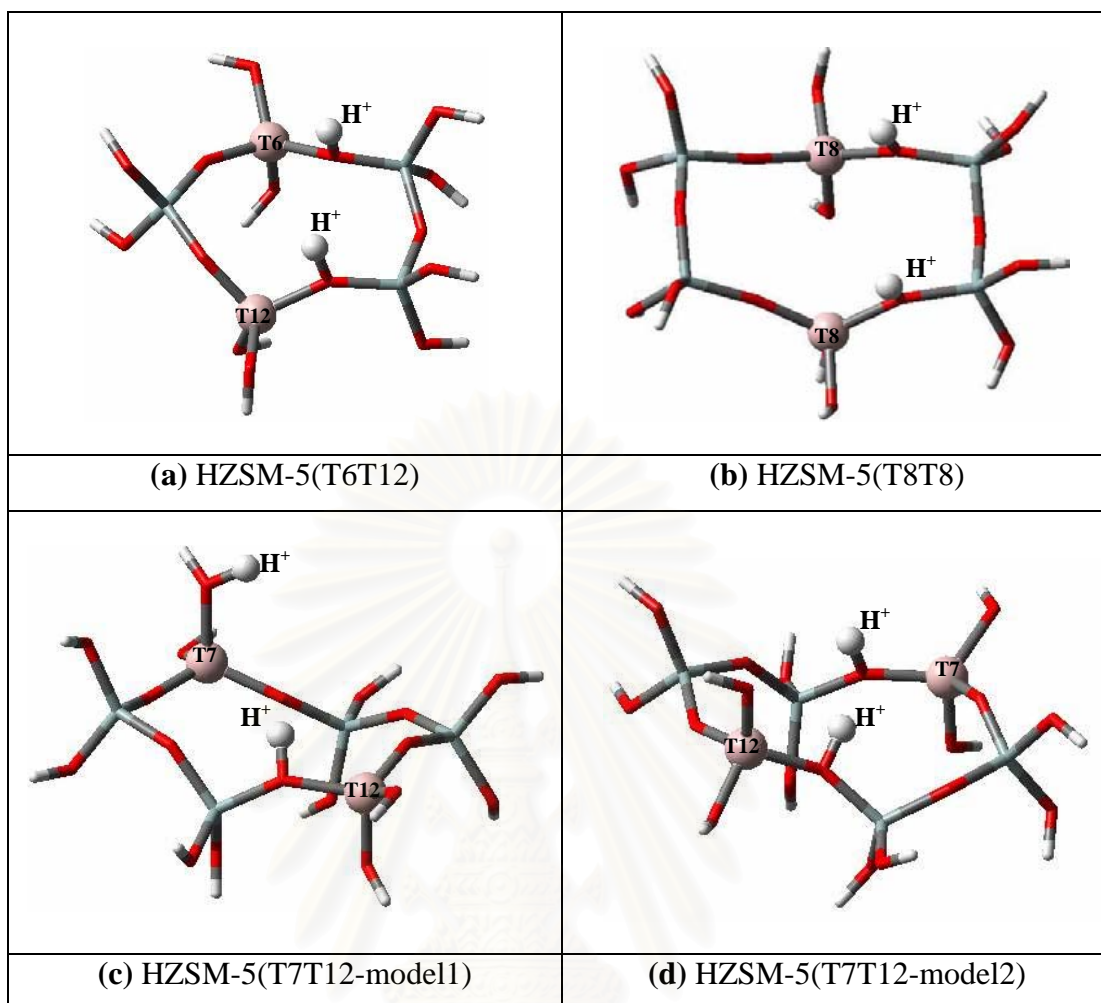


Fig. 4.2 Cluster models were obtained from the simulated HZSM-5 structure and then adjusted to the quantum calculations; (a) HZSM-5(T6T12), (b) HZSM-5(T8T8), (c) HZSM-5(T7T12(model1)), and (d) HZSM-5(T7T12(model2)).



4.2.2 CuZSM-5 Cluster Model

Cluster models of CuZSM-5 are classified into two groups as one- and two-ion exchanged CuZSM-5. For one-ion exchanged CuZSM-5, 1 H⁺ were replaced by 1 Cu⁺ or 2 H⁺ were replaced by 1 Cu²⁺. For two-ion exchanged CuZSM-5, 2 H⁺ were replaced by 2 Cu⁺. Only positions of H⁺, Cu⁺, and Cu²⁺ were optimized. Totally, 16 CuZSM-5 clusters were optimized and list of these clusters was given in Table 4.2.

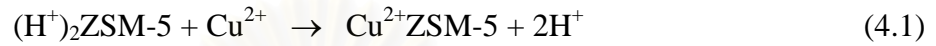
Table 4.2 CuZSM-5 exchanged sites were optimized partially using B3LYP/6-31G(d,p).

Cu species	one-ion exchanged CuZSM-5
1 Cu ²⁺	Cu ²⁺ ZSM-5(T6T12)
	Cu ²⁺ ZSM-5(T8T8)
	Cu ²⁺ ZSM-5(T7T12-model1)
	Cu ²⁺ ZSM-5(T7T12-model2)
1 Cu ⁺	Cu ⁺ ZSM-5(T6T12, Cu ⁺ at T6)
	Cu ⁺ ZSM-5(T6T12, Cu ⁺ at T12)
	Cu ⁺ ZSM-5(T8T8, Cu ⁺ at T8)
	Cu ⁺ ZSM-5(T8T8, Cu ⁺ at T8')
	Cu ⁺ ZSM-5(T7T12-model1, Cu ⁺ at T7)
	Cu ⁺ ZSM-5(T7T12-model1, Cu ⁺ at T12)
	Cu ⁺ ZSM-5(T7T12-model2, Cu ⁺ at T7)
	Cu ⁺ ZSM-5(T7T12-model2, Cu ⁺ at T12)
Cu species	two-ion exchanged CuZSM-5
2 Cu ⁺	Cu ⁺ ZSM-5(T6T12)
	Cu ⁺ ZSM-5(T8T8)
	Cu ⁺ ZSM-5(T7T12-model1)
	Cu ⁺ ZSM-5(T7T12-model2)

4.2.3 Exchanged Energy

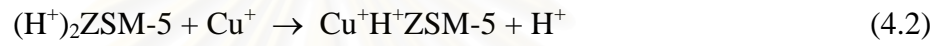
Exchanged energy (ΔE_{exch}) of the one- and two-ion exchanged CuZSM-5 at T6T12, T8T8, T7T12-model1, and T7T12-model2 exchanged sites were calculated as followed:

(i) *Exchange of 1 Cu²⁺ in ZSM-5*



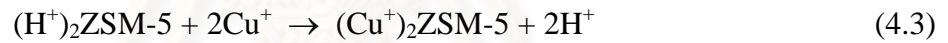
$$\Delta E_{\text{exch}} = E[\text{Cu}^{2+}\text{ZSM-5}] - E[(\text{H}^+)_2\text{ZSM-5}] - E[\text{Cu}^{2+}]$$

(ii) *Exchange of 1 Cu⁺ in ZSM-5*



$$\Delta E_{\text{exch}} = E[\text{Cu}^+\text{H}^+\text{ZSM-5}] - E[(\text{H}^+)_2\text{ZSM-5}] - E[\text{Cu}^+]$$

(iii) *Exchange of 2 Cu⁺ in ZSM-5*



$$\Delta E_{\text{exch}} = E[(\text{Cu}^+)_2\text{ZSM-5}] - E[(\text{H}^+)_2\text{ZSM-5}] - 2E[\text{Cu}^+].$$

4.2.4 Autoreduction

Autoreduction Energy (ΔE_{auto}) of Cu²⁺ to Cu⁺ in ZSM-5 at T6T12, T8T8, T7T12-model1, and T7T12-model2 exchanged sites were determined using:



$$\Delta E_{\text{auto}} = E[\text{Cu}^+\text{H}^+\text{ZSM-5}] - E[\text{Cu}^{2+}\text{ZSM-5}] - 1/2E[\text{H}_2].$$

CHAPTER 5

RESULTS

Structures of HZSM-5, one-ion exchanged Cu^{2+} ZSM-5, one- and two-ion exchanged Cu^+ ZSM-5 at T6T12, T8T8, T7T12-model1 and T7T12-model2 exchanged sites obtained from B3LYP/6-31G(d,p) were presented in Figs. 5.1-5.20. Important geometrical parameters and total energies were given in the figures for HZSM-5 and in Tables 5.1-5.13 for the one- and two-ion exchanged CuZSM-5.



สถาบันวิทยบริการ
จุฬาลงกรณ์มหาวิทยาลัย

5.1 HZSM-5

5.1.1 Optimized Geometries of HZSM-5

5.1.1.1 T6T12

Fig. 5.1 shows optimized structure of HZSM-5(T6T12). The O-H bond distance of 0.96 Å and T-O-H bond angle of 115.33° were obtained. The O-H⁺ distance of 0.99 Å was yielded.

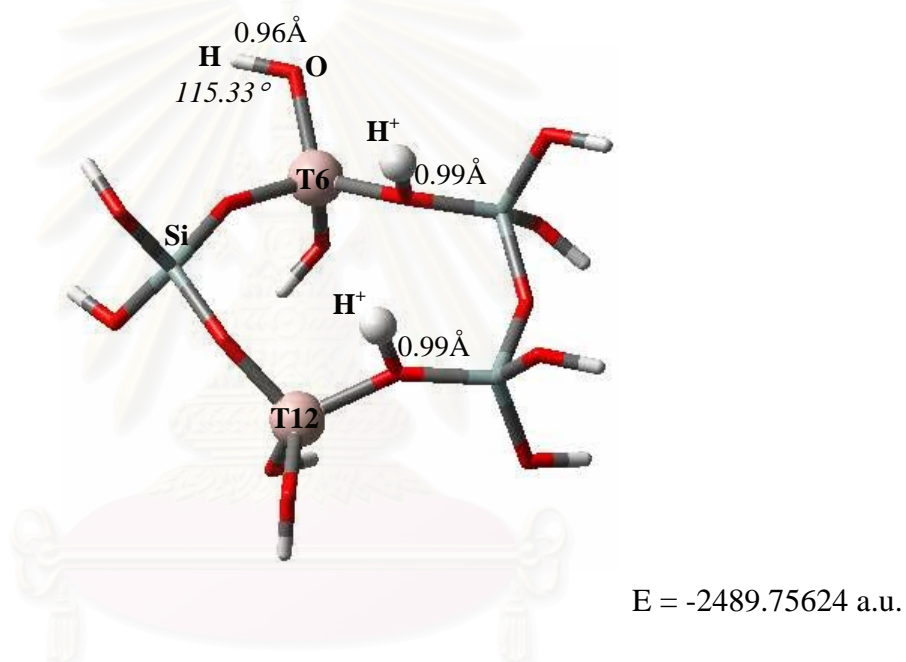


Fig. 5.1 Optimized structures of HZSM-5(T6T12).

สถาบันวิทยบริการ
จุฬาลงกรณ์มหาวิทยาลัย

5.1.1.2 T8T8

Fig. 5.2 shows optimized structure of HZSM-5(T8T8). The O-H bond distance of 0.96 Å and T-O-H bond angle of 116.00° were obtained. The O-H⁺ distance of 0.98 Å was yielded.

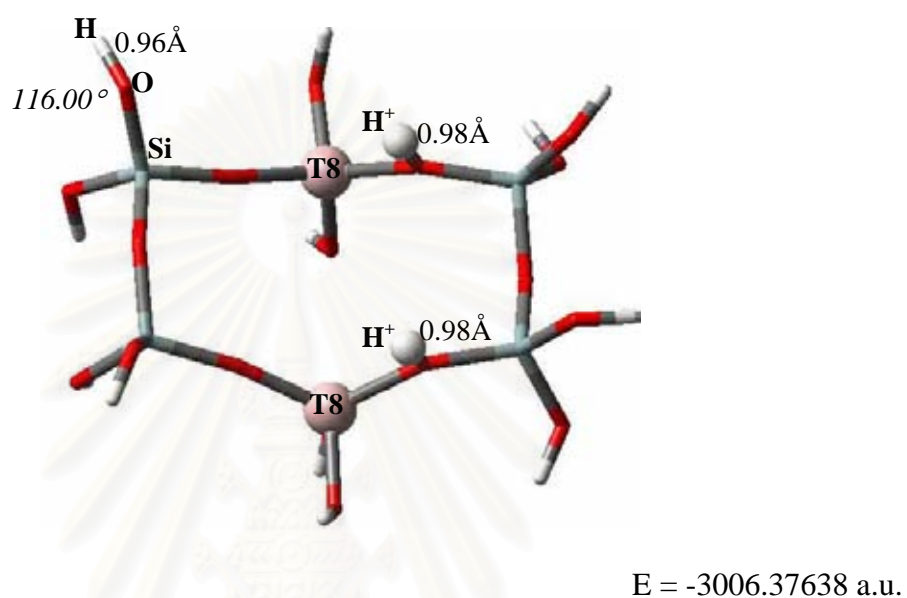
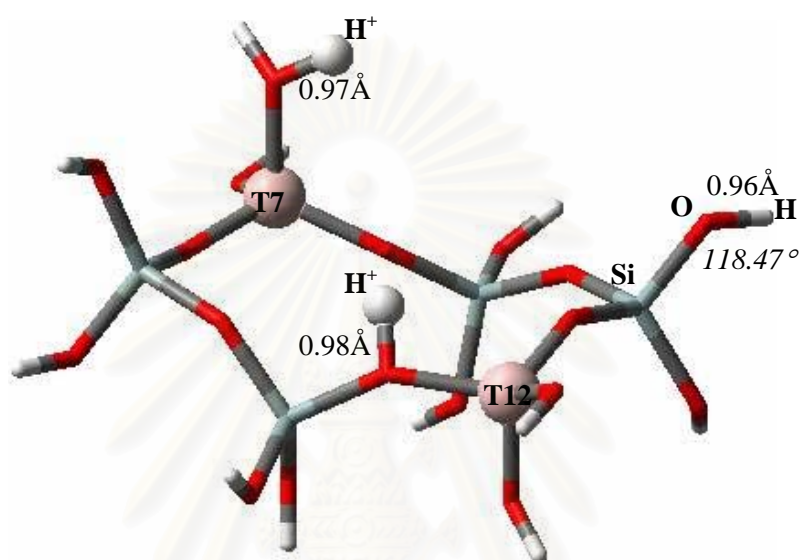


Fig. 5.2 Optimized structures of HZSM-5(T8T8).

5.1.1.3 T7T12-modell

Fig. 5.3 shows optimized structure of HZSM-5(T7T12-modell1). The O-H bond distance of 0.96 Å and T-O-H bond angle of 118.47° were obtained. The O-H⁺ distances of 0.97 and 0.98 Å were yielded.



E = -3006.41297 a.u.

Fig. 5.3 Optimized structures of HZSM-5(T7T12-modell1).

สถาบันวิทยบริการ
จุฬาลงกรณ์มหาวิทยาลัย

5.1.1.4 T7T12-model2

Fig. 5.4 shows optimized structure of HZSM-5(T7T12-model2). The O-H bond distance of 0.96 Å and T-O-H bond angle of 118.98° were obtained. The O-H⁺ distance of 0.98 Å was yielded.

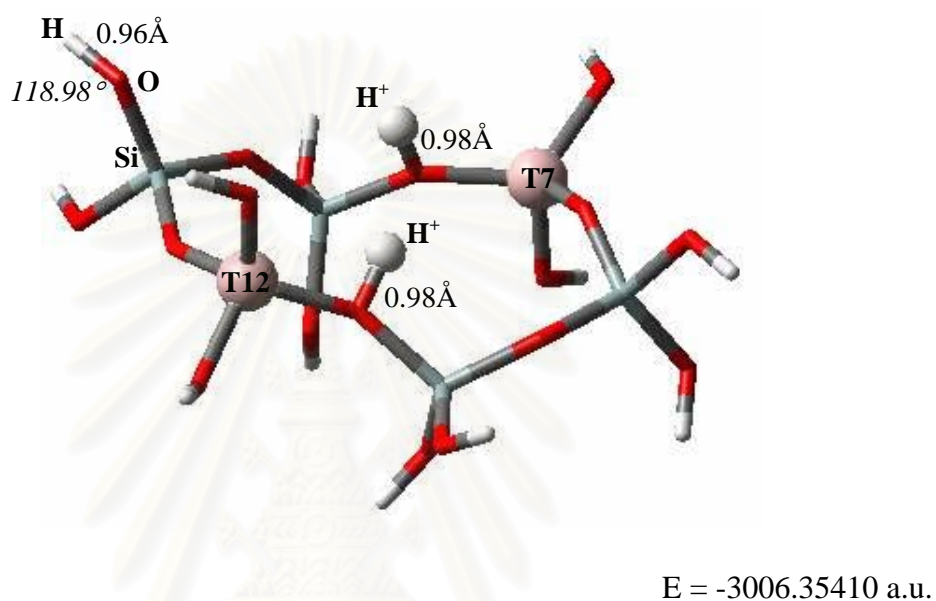


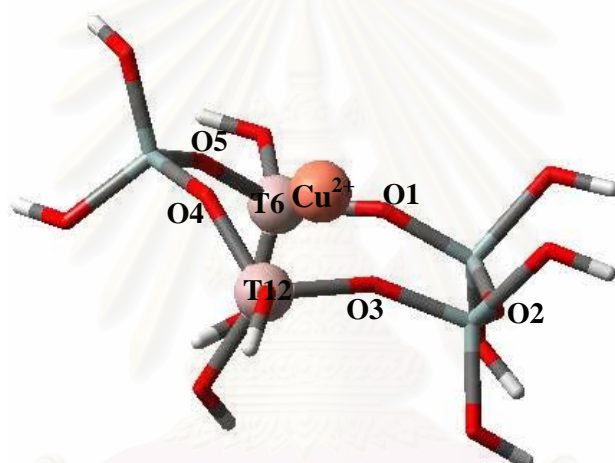
Fig. 5.4 Optimized structures of HZSM-5(T7T12-model2).

5.2 One-ion Exchanged Cu^{2+} ZSM-5

5.2.1 Optimized Geometries of One-ion Exchanged Cu^{2+} ZSM-5

5.2.1.1 T6T12

The structure of one-ion exchanged Cu^{2+} ZSM-5 at T6T12 was shown in Fig. 5.5, and the distances between Cu^{2+} and O in ring of T6T12 are given in Table 5.1. From Table 5.1, Cu^{2+} -O distances are in the range between 1.96 and 3.20 Å. In this range, only 2 distances, Cu-O1 and Cu-O3 are less than 2.00 Å.



E = -4128.95538 a.u.

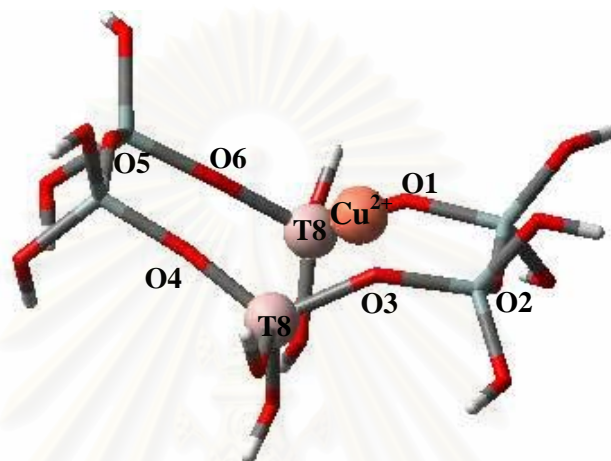
Fig. 5.5 Optimized structures of one-ion exchanged Cu^{2+} ZSM-5(T6T12).

Table 5.1 Cu^{2+} -O distances of one-ion exchanged Cu^{2+} ZSM-5(T6T12).

parameters	distance (Å)
Cu^{2+} -O1	1.96
Cu^{2+} -O2	3.20
Cu^{2+} -O3	1.99
Cu^{2+} -O4	2.13
Cu^{2+} -O5	2.29

5.2.1.2 T8T8

The structure of one-ion exchanged $\text{Cu}^{2+}\text{ZSM-5}$ at T8T8 was shown in Fig. 5.6, and the distances between Cu^{2+} and O in ring of T8T8 are given in Table 5.2. From Table 5.2, Cu^{2+} -O distances are in the range between 1.92 and 4.17 Å. In this range, only 2 distances, Cu-O1 and Cu-O3 are less than 2.00 Å.



E = -4645.51230 a.u.

Fig. 5.6 Optimized structures of one-ion exchanged $\text{Cu}^{2+}\text{ZSM-5(T8T8)}$.

Table 5.2 Cu^{2+} -O distances of one-ion exchanged $\text{Cu}^{2+}\text{ZSM-5(T8T8)}$.

parameters	distance (Å)
Cu^{2+} -O1	1.93
Cu^{2+} -O2	2.44
Cu^{2+} -O3	1.92
Cu^{2+} -O4	3.09
Cu^{2+} -O5	4.17
Cu^{2+} -O6	3.07

5.2.1.3 T7T12-modell

The structure of one-ion exchanged $\text{Cu}^{2+}\text{ZSM-5}$ at T7T12-modell1 was shown in Fig. 5.7, and the distances between Cu^{2+} and O in ring of T7T12-modell1 are given in Table 5.3. From Table 5.3, Cu^{2+} -O distances are in the range between 1.95 and 3.13 Å. In this range, only 2 distances, Cu-O1 and Cu-O4 are less than 2.00 Å.

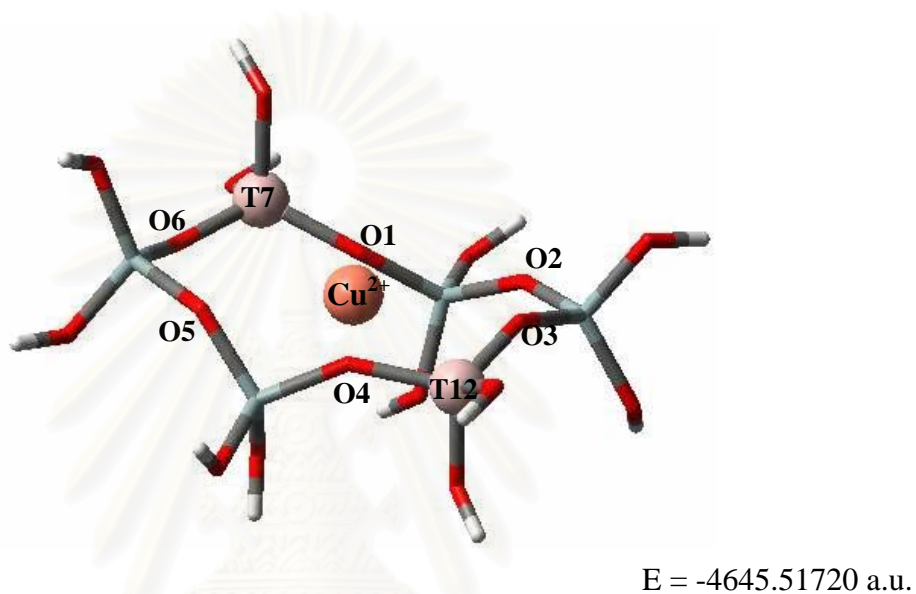


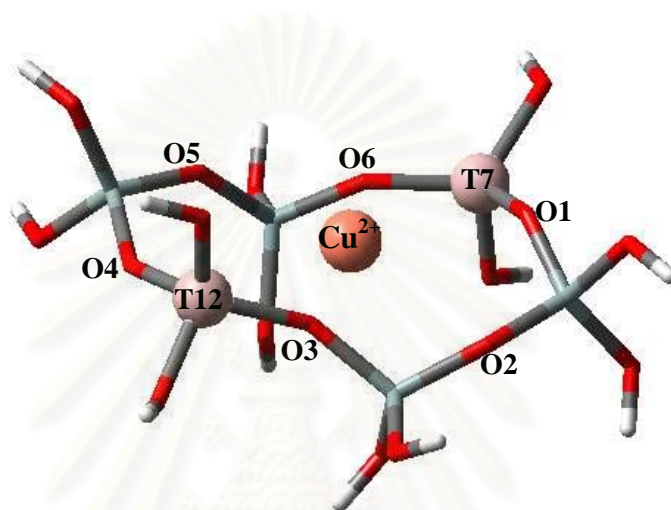
Fig. 5.7 Optimized structures of one-ion exchanged $\text{Cu}^{2+}\text{ZSM-5}$ (T7T12-modell1).

Table 5.3 Cu^{2+} -O distances of one-ion exchanged $\text{Cu}^{2+}\text{ZSM-5}$ (T7T12-modell1).

parameters	distance (Å)
Cu^{2+} -O1	1.95
Cu^{2+} -O2	3.07
Cu^{2+} -O3	2.79
Cu^{2+} -O4	1.96
Cu^{2+} -O5	2.64
Cu^{2+} -O6	3.13

5.2.1.4 T7T12-model2

The structure of one-ion exchanged $\text{Cu}^{2+}\text{ZSM-5}$ at T7T12-model2 was shown in Fig. 5.8, and the distances between Cu^{2+} and O in ring of T7T12-model2 are given in Table 5.4. From Table 5.4, Cu^{2+} -O distances are in the range between 1.95 and 3.27 Å. In this range, only 1 distances, Cu-O3 is less than 2.00 Å.



E = -4645.49814 a.u.

Fig. 5.8 Optimized structures of one-ion exchanged $\text{Cu}^{2+}\text{ZSM-5}$ (T7T12-model2).

Table 5.4 Cu^{2+} -O distances of one-ion exchanged $\text{Cu}^{2+}\text{ZSM-5}$ (T7T12-model2).

parameters	distance (Å)
Cu^{2+} -O1	2.74
Cu^{2+} -O2	2.99
Cu^{2+} -O3	1.95
Cu^{2+} -O4	3.27
Cu^{2+} -O5	2.73
Cu^{2+} -O6	2.02

5.2.2 Exchanged Energies of One-ion Exchanged Cu²⁺ZSM-5

Exchanged energies (ΔE_{exch}) of Cu²⁺ on ZSM-5 at various exchanged sites are listed in Table 5.5. All ΔE_{exch} are shown positively. Only exchange of Cu²⁺ at T6T12 site has the ΔE_{exch} less than 10.00 kcal/mol.

Table 5.5 Exchanged energies of Cu²⁺ exchanged in T6T12, T8T8, T7T12-model1, and T7T12-model2 exchanged site.

exchanged sites	ΔE_{exch} (kcal/mol)
T6T12	9.19
T8T8	48.86
T7T12-model1	68.75
T7T12-model2	43.77

5.3 One-ion Exchanged $\text{Cu}^+\text{ZSM-5}$

5.3.1 Optimized Geometries of One-ion Exchanged $\text{Cu}^+\text{ZSM-5}$

5.3.1.1 T6T12

The structures of one-ion exchanged $\text{Cu}^+\text{ZSM-5}$ at T6T12 were shown in Fig. 5.9, and 5.10, respectively, and distances between Cu^+ and O in ring of the T6T12 are given in Table 5.6. From Table 5.6, exchange of Cu^+ at T6, $\text{Cu}^+\text{-O}$ distances are in the range between 1.89 and 5.33 Å. In this range, only 1 distance, $\text{Cu}^+\text{-O}'1$ is less than 2.00 Å, and exchange of Cu^+ at T12, $\text{Cu}^+\text{-O}$ distances are in the range between 1.93 and 3.91 Å. In this range, only 1 distance, $\text{Cu}^+\text{-O4}$ is less than 2.00 Å.

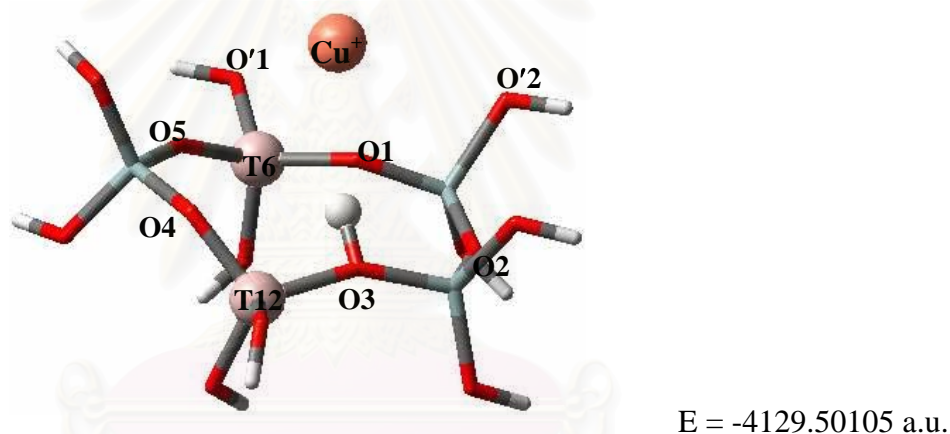


Fig. 5.9 Optimized structures of one-ion exchanged $\text{Cu}^+\text{ZSM-5}$ (T6T12, Cu^+ at T6).

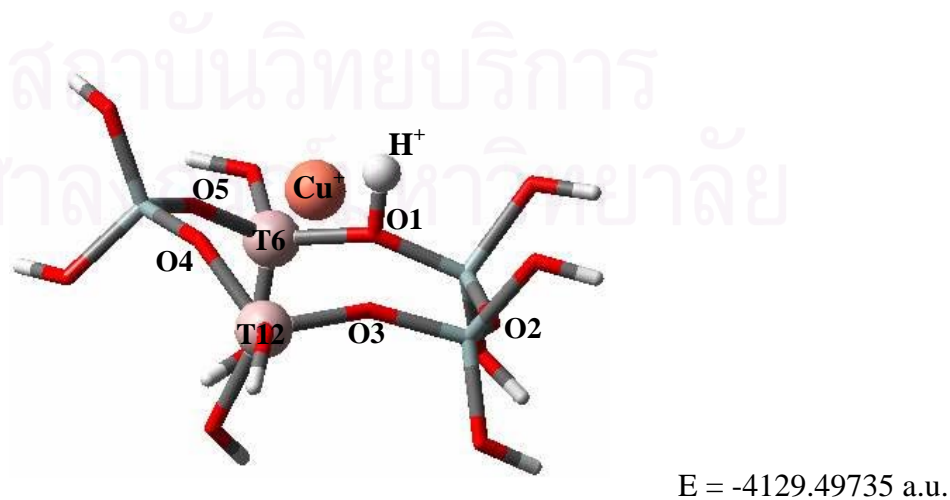


Fig. 5.10 Optimized structures of one-ion exchanged $\text{Cu}^+\text{ZSM-5}$ (T6T12, Cu^+ at T12).

Table 5.6 Distances of Cu⁺-O and H⁺-O of one-ion exchanged Cu⁺ZSM-5(T6T12) when Cu⁺ at T6 and T12 sites.

Cu⁺ at T6

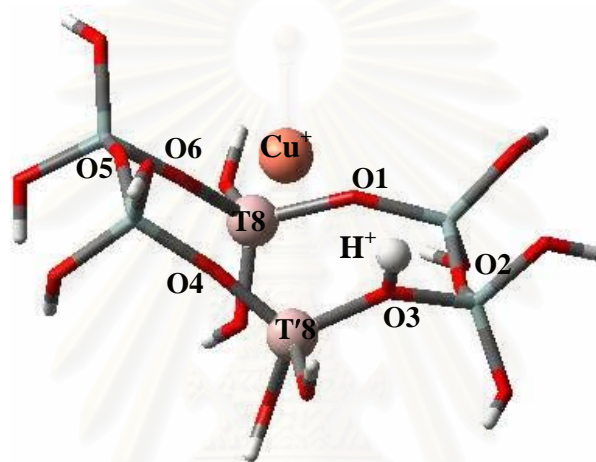
parameters	distance (Å)
H ⁺ -O3	0.99
Cu ⁺ -O1	2.17
Cu ⁺ -O2	4.45
Cu ⁺ -O3	5.14
Cu ⁺ -O4	5.33
Cu ⁺ -O5	3.32
Cu ⁺ -O'1	1.89

Cu⁺ at T12

parameters	distance (Å)
H ⁺ -O1	0.98
Cu ⁺ -O1	3.34
Cu ⁺ -O2	3.91
Cu ⁺ -O3	2.03
Cu ⁺ -O4	1.93
Cu ⁺ -O5	3.41

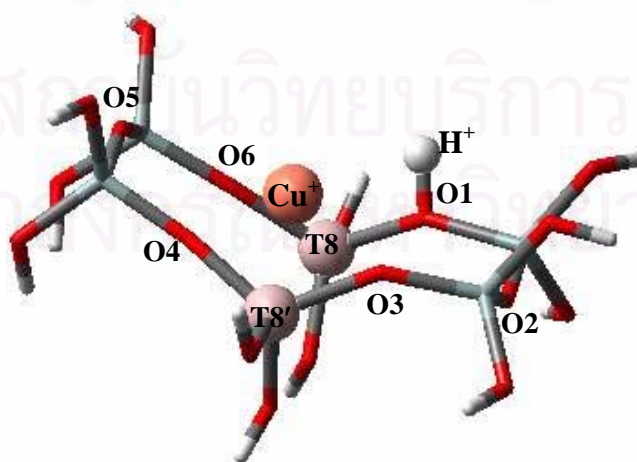
5.3.1.2 T8T8

The structures of one-ion exchanged $\text{Cu}^+\text{ZSM-5}$ at T8T8 were shown in Fig. 5.11, and 5.12, respectively, and distances between Cu^+ and O in ring of the T8T8 are given in Table 5.7. From Table 5.7, exchange of Cu^+ at T8, $\text{Cu}^+\text{-O}$ distances are in the range between 1.96 and 3.77 Å. In this range, only 1 distance, $\text{Cu}^+\text{-O6}$ is less than 2.00 Å, and exchange of Cu^+ at T'8, $\text{Cu}^+\text{-O}$ distances are in the range between 1.75 and 3.85 Å. In this range, only 2 distances, $\text{Cu}^+\text{-O4}$ and $\text{Cu}^+\text{-O4}$ are less than 2.00 Å.



E = -4646.10525 a.u.

Fig. 5.11 Optimized structures of one-ion exchanged $\text{Cu}^+\text{ZSM-5(T8T8, Cu}^+\text{ at T8)}$.



E = -4646.09282 a.u.

Fig. 5.12 Optimized structures of one-ion exchanged $\text{Cu}^+\text{ZSM-5(T8T8, Cu}^+\text{ at T'8)}$.

Table 5.7 Distances of Cu⁺-O and H⁺-O of one-ion exchanged Cu⁺ZSM-5(T8T8) when Cu⁺ at T8 and T'8 sites.

Cu⁺ at T8

parameters	distance (Å)
H ⁺ -O3	0.98
Cu ⁺ -O1	2.02
Cu ⁺ -O2	3.77
Cu ⁺ -O3	3.36
Cu ⁺ -O4	3.30
Cu ⁺ -O5	3.25
Cu ⁺ -O6	1.96

Cu⁺ at T'8

parameters	distance (Å)
H ⁺ -O1	0.98
Cu ⁺ -O1	3.56
Cu ⁺ -O2	3.85
Cu ⁺ -O3	1.92
Cu ⁺ -O4	1.75
Cu ⁺ -O5	3.27
Cu ⁺ -O6	3.39

5.3.1.3 T7T12-modell

The structures of one-ion exchanged $\text{Cu}^+\text{ZSM-5}$ at T7T12-modell1 were shown in Fig. 5.13, and 5.14, respectively, and distances between Cu^+ and O in ring of the T7T12-modell1 are given in Table 5.8. From Table 5.8, exchange of Cu^+ at T7, $\text{Cu}^+\text{-O}$ distances are in the range between 1.89 and 4.47 Å. In this range, only 2 distance, $\text{Cu}^+\text{-O}'1$ and $\text{Cu}^+\text{-O1}$ are less than 2.00 Å, and exchange of Cu^+ at T12, $\text{Cu}^+\text{-O}$ distances are in the range between 1.98 and 3.51 Å. In this range, only 1 distance, $\text{Cu}^+\text{-O4}$ is less than 2.00 Å.

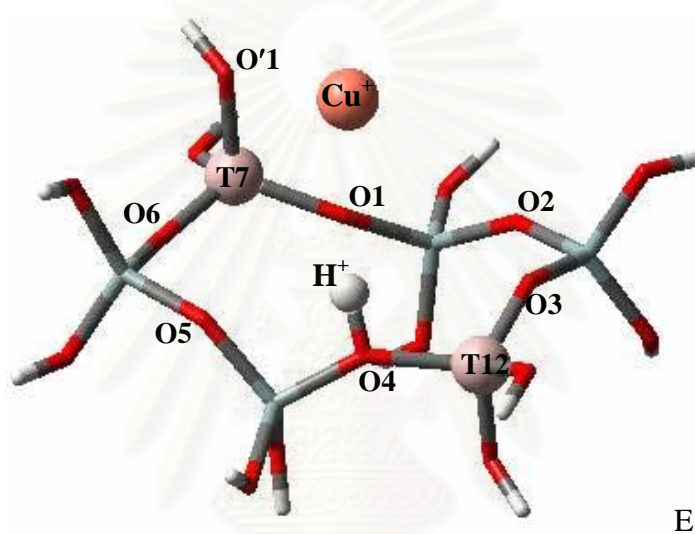


Fig. 5.13 Optimized structures of one-ion exchanged $\text{Cu}^+\text{ZSM-5}$ (T7T12-modell1, Cu^+ at T7).

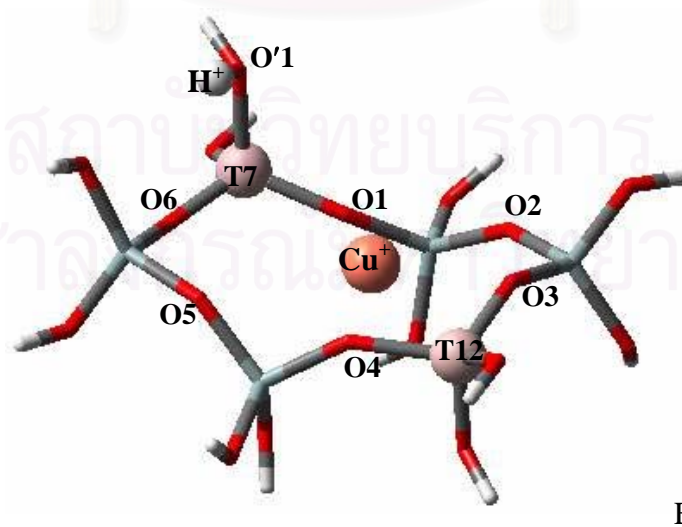


Fig. 5.14 Optimized structures of one-ion exchanged $\text{Cu}^+\text{ZSM-5}$ (T7T12-modell1, Cu^+ at T12).

Table 5.8 Distances of Cu⁺-O and H⁺-O of one-ion exchanged Cu⁺ZSM-5(T7T12-model1) when Cu⁺ at T7 and T12 sites.

Cu⁺ at T7

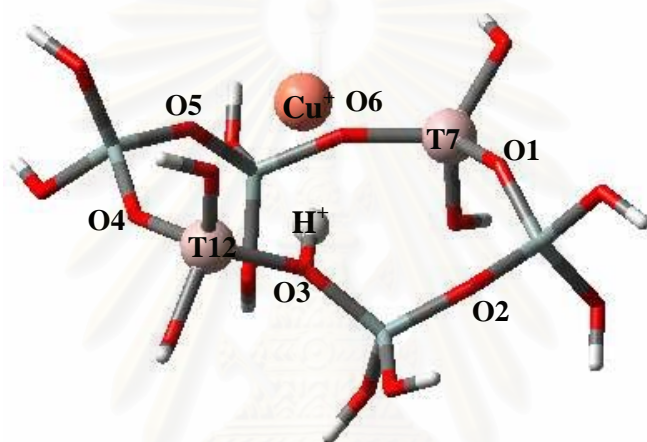
parameters	distance (Å)
H ⁺ -O4	0.97
Cu ⁺ -O1	1.98
Cu ⁺ -O2	2.23
Cu ⁺ -O3	4.19
Cu ⁺ -O4	4.53
Cu ⁺ -O5	4.47
Cu ⁺ -O6	3.57
Cu-O'1	1.89

Cu⁺ at T12

parameters	distance (Å)
H ⁺ -O'1	0.98
Cu ⁺ -O1	2.02
Cu ⁺ -O2	2.75
Cu ⁺ -O3	2.40
Cu ⁺ -O4	1.98
Cu ⁺ -O5	2.99
Cu ⁺ -O6	3.51

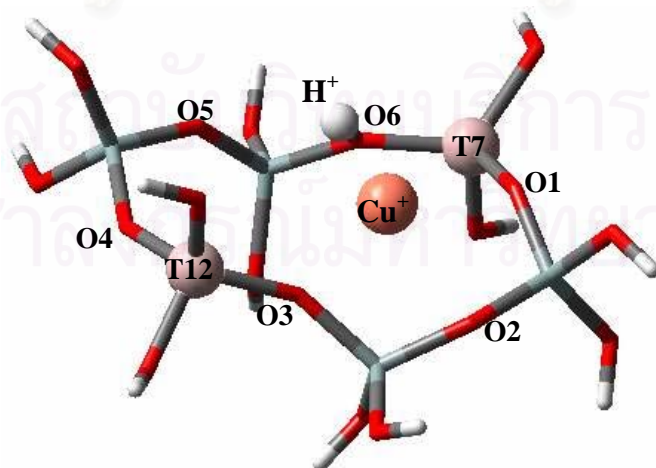
5.3.1.4 T7T12-model2

The structures of one-ion exchanged $\text{Cu}^+\text{ZSM-5}$ at T7T12-model2 were shown in Fig. 5.15, and 5.16, respectively, and distances between Cu^+ and O in ring of the T7T12-model2 are given in Table 5.9. From Table 5.9, exchange of Cu^+ at T7, $\text{Cu}^+\text{-O}$ distances are in the range between 1.93 and 4.19 Å. In this range, only 1 distance, $\text{Cu}^+\text{-O6}$ is less than 2.00 Å, and exchange of Cu^+ at T12, $\text{Cu}^+\text{-O}$ distances are in the range between 1.99 and 3.98 Å. In this range, only 1 distance, $\text{Cu}^+\text{-O3}$ is less than 2.00 Å.



E = -4646.05932 a.u.

Fig. 5.15 Optimized structures of one-ion exchanged $\text{Cu}^+\text{ZSM-5}$ (T7T12-model2, Cu^+ at T7).



E = -4646.06599 a.u.

Fig. 5.16 Optimized structures of one-ion exchanged $\text{Cu}^+\text{ZSM-5}$ (T7T12-model2, Cu^+ at T12).

Table 5.9 Distances of Cu⁺-O and H⁺-O of one-ion exchanged Cu⁺ZSM-5(T7T12-model2) when Cu⁺ at T7 and T12 sites.

Cu⁺ at T7

parameters	distance (Å)
H ⁺ -O6	0.99
Cu-O1	3.31
Cu-O2	4.19
Cu-O3	3.05
Cu-O4	3.37
Cu-O5	2.16
Cu-O6	1.93

Cu⁺ at T12

parameters	distance (Å)
H ⁺ -O3	1.00
Cu-O1	2.19
Cu-O2	2.26
Cu-O3	1.99
Cu-O4	3.98
Cu-O5	3.71
Cu-O6	2.72

5.3.2 Exchanged Energy of One-ion Exchanged Cu⁺ZSM-5

Exchanged energy (ΔE_{exch}) of one-ion exchanged Cu⁺ZSM-5 at various exchanged sites are given in Table 5.10. ΔE_{exch} are in the range of 66.62-105.72 kcal/mol. The lowest is exchange of Cu⁺ at T12 in T7T12-model1.

Table 5.10 Exchanged energy of one-ion exchanged Cu⁺ZSM-5 at T6T12, T8T8, T7T12-model1, and T7T12-model2 exchanged site.

exchanged sites	ΔE_{exch} (kcal/mol)
T6T12, Cu ⁺ at T6	72.85
T6T12, Cu ⁺ at T12	75.17
T8T8, Cu ⁺ at T8	82.85
T8T8, Cu ⁺ at T8'	90.65
T7T12-model1, Cu ⁺ at T7	105.72
T7T12-model1, Cu ⁺ at T12	66.62
T7T12-model2, Cu ⁺ at T7	93.50
T7T12-model2, Cu ⁺ at T12	97.70

5.4 Two-ion Exchanged Cu⁺ZSM-5

5.4.1 Optimized Geometries of Two-ion Exchanged Cu⁺ZSM-5

5.4.1.1 T6T12

The structure of two-ion exchanged Cu⁺ZSM-5 at T6T12 was shown in Fig. 5.17, and distances between Cu⁺ and Cu⁺, between Cu⁺ and O in ring of the T6T12 are given in Table 5.11. From Table 5.11, Cu⁺-O distances are in the range between 1.96 and 4.85 Å. In this range, only 1 distance, Cu²⁺-O6 is less than 2.00 Å, and 2 distances, Cu¹⁺-O1 and Cu¹⁺-O3 are equal to 2.00 Å.

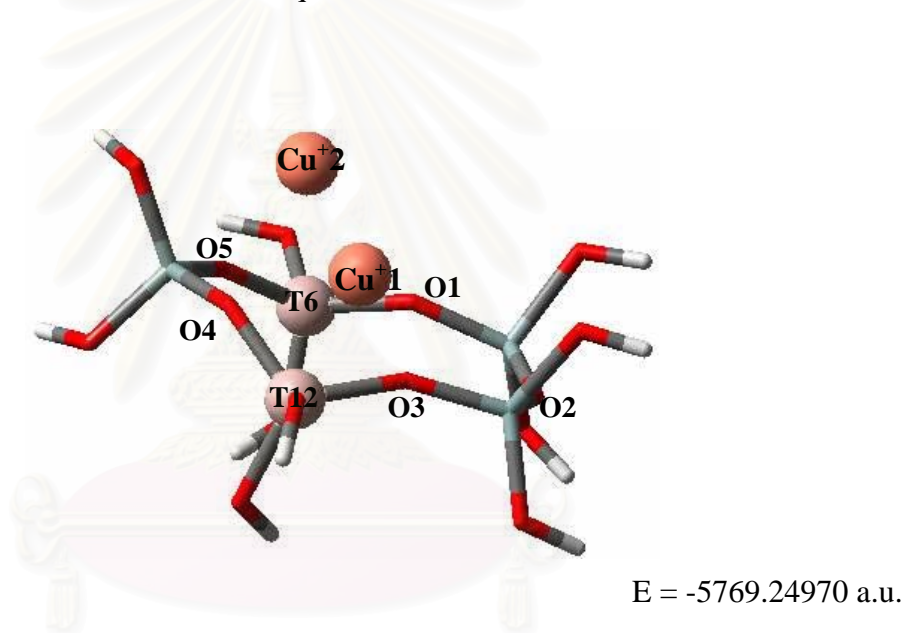


Fig. 5.17 Optimized structures of two-ion exchanged Cu⁺ZSM-5(T6T12).

สถาบันวิทยบริการ
จุฬาลงกรณ์มหาวิทยาลัย

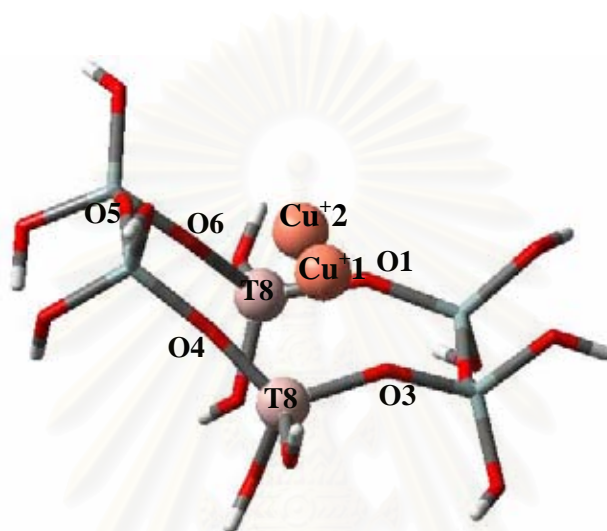
Table 5.11 Cu⁺-Cu⁺ and Cu⁺-O distances of two-ion exchanged Cu⁺ZSM-5(T6T12).

parameters	distance (Å)
Cu ⁺ 1-Cu ⁺ 2	2.39
Cu ⁺ 1-O1	2.00
Cu ⁺ 1-O2	3.17
Cu ⁺ 1-O3	2.00
Cu ⁺ 1-O4	2.27
Cu ⁺ 1-O5	2.50
Cu ⁺ 2-O1	2.55
Cu ⁺ 2-O2	4.85
Cu ⁺ 2-O3	4.37
Cu ⁺ 2-O4	3.60
Cu ⁺ 2-O5	1.96

สถาบันวิทยบริการ
จุฬาลงกรณ์มหาวิทยาลัย

5.4.1.2 T8T8

The structure of two-ion exchanged $\text{Cu}^+\text{ZSM-5}$ at T8T8 was shown in Fig. 5.18, and distances between Cu^+ and Cu^+ , between Cu^+ and O in ring of the T8T8 are given in Table 5.12. From Table 5.12, $\text{Cu}^+\text{-O}$ distances are in the range between 1.94 and 3.90 Å. In this range, only 1 distance, $\text{Cu}^{+2}\text{-O6}$ is less than 2.00 Å.



E = -6285.83162 a.u.

Fig. 5.18 Optimized structures of two-ion exchanged $\text{Cu}^+\text{ZSM-5(T8T8)}$.

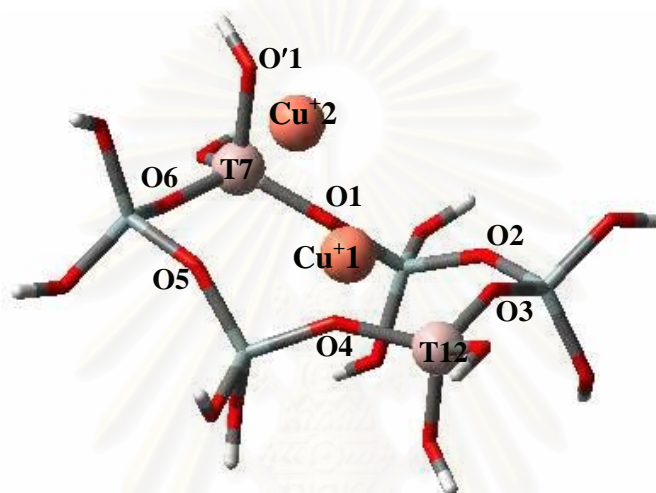
สถาบันวิทยบริการ
จุฬาลงกรณ์มหาวิทยาลัย

Table 5.12 Cu⁺-Cu⁺ and Cu⁺-O distances of two-ion exchanged Cu⁺ZSM-5(T8T8).

parameters	distance (Å)
Cu ⁺ 1-Cu ⁺ 2	2.28
Cu ⁺ 1-O1	3.22
Cu ⁺ 1-O2	3.25
Cu ⁺ 1-O3	2.02
Cu ⁺ 1-O4	2.02
Cu ⁺ 1-O5	3.69
Cu ⁺ 1-O6	3.23
Cu ⁺ 2-O1	2.10
Cu ⁺ 2-O2	3.51
Cu ⁺ 2-O3	3.73
Cu ⁺ 2-O4	3.72
Cu ⁺ 2-O5	3.90
Cu ⁺ 2-O6	1.94

5.4.1.3 T7T12-modell

The structure of two-ion exchanged $\text{Cu}^+\text{ZSM-5}$ at T7T12-modell was shown in Fig. 5.19, and distances between Cu^+ and Cu^+ , between Cu^+ and O in ring of the T7T12-modell are given in Table 5.13. From Table 5.13, $\text{Cu}^+\text{-O}$ distances are in the range between 1.98 and 4.28 Å. In this range, there are 3 distances; $\text{Cu}^+\text{1-O1}$, $\text{Cu}^+\text{1-O4}$, and $\text{Cu}^+\text{2-O'1}$ are less than 2.00 Å.



E = -6285.87005 a.u.

Fig. 5.19 Optimized structures of two-ion exchanged $\text{Cu}^+\text{ZSM-5}$ (T7T12-modell).

สถาบันวิทยบริการ
จุฬาลงกรณ์มหาวิทยาลัย

Table 5.13 Cu^+-Cu^+ and Cu^+-O distances of two-ion exchanged $\text{Cu}^+\text{ZSM-5(T7T12-model1)}$.

parameters	distance (Å)
$\text{Cu}^+1-\text{Cu}^+2$	2.34
$\text{Cu}^+1-\text{O}1$	1.98
$\text{Cu}^+1-\text{O}2$	2.88
$\text{Cu}^+1-\text{O}3$	2.56
$\text{Cu}^+1-\text{O}4$	1.99
$\text{Cu}^+1-\text{O}5$	2.84
$\text{Cu}^+1-\text{O}6$	3.34
$\text{Cu}^+2-\text{O}1$	2.67
$\text{Cu}^+2-\text{O}2$	4.27
$\text{Cu}^+2-\text{O}3$	4.28
$\text{Cu}^+2-\text{O}4$	3.65
$\text{Cu}^+2-\text{O}5$	3.10
$\text{Cu}^+2-\text{O}6$	2.88
$\text{Cu}^+2-\text{O}'1$	1.88

5.4.1.4 T7T12-model2

The structure of two-ion exchanged $\text{Cu}^+\text{ZSM-5}$ at T7T12-model2 was shown in Fig. 5.20, and distances between Cu^+ and Cu^+ , between Cu^+ and O in ring of the T7T12-model2 are given in Table 5.14. From Table 5.14, $\text{Cu}^+\text{-O}$ distances are in the range between 2.01 and 4.50 Å. In this range, there are 3 distances, $\text{Cu}^+\text{-O3}$ is 2.01 Å, $\text{Cu}^+\text{-O5}$, and $\text{Cu}^+\text{-O6}$ are 2.02 Å.

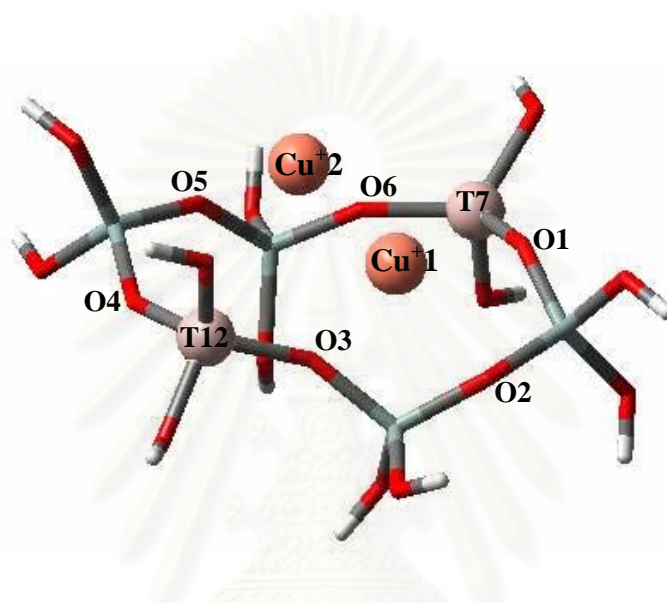


Fig. 5.20 Optimized structures of two-ion exchanged $\text{Cu}^+\text{ZSM-5}$ (T7T12-model2).

Table 5.14 Cu⁺-Cu⁺ and Cu⁺-O distances of two-ion exchanged Cu⁺ZSM-5(T7T12-model2).

parameters	distance (Å)
Cu ⁺ 1-Cu ⁺ 2	2.23
Cu ⁺ 1-O1	2.16
Cu ⁺ 1-O2	2.27
Cu ⁺ 1-O3	2.01
Cu ⁺ 1-O4	3.99
Cu ⁺ 1-O5	3.68
Cu ⁺ 1-O6	2.66
Cu ⁺ 2-O1	3.60
Cu ⁺ 2-O2	4.50
Cu ⁺ 2-O3	3.26
Cu ⁺ 2-O4	3.32
Cu ⁺ 2-O5	2.02
Cu ⁺ 2-O6	2.02

5.3.2 Exchanged Energies of Two-ion Exchanged Cu⁺ZSM-5

Exchanged energies (ΔE_{exch}) of 2 Cu⁺ on ZSM-5 at various exchanged sites are listed in Table 5.15. Very high ΔE_{exch} were observed from exchange of Cu⁺ in ZSM-5.

Table 5.15 Exchanged energies of 2 Cu⁺ exchanged in T6T12, T8T8, T7T12-model1, and T7T12-model2 exchanged site.

exchanged sites	ΔE_{exch} (kcal/mol)
T6T12	143.29
T8T8	167.27
T7T12-model1	166.12
T7T12-model2	164.94

5.5 Autoreduction Energy of Cu^{2+} to Cu^+ in ZSM-5 at T6T12, T8T8, T7T12-model1, and T7T12-model2 Exchanged Site

Autoreduction energy (ΔE_{auto}) of Cu species resided at various exchanged sites were given in Table 5.16.

Table 5.16 Autoreduction energy of Cu^{2+} in the cavity of ZSM-5 at T6T12, T8T8, T7T12-model1, and T7T12-model2 exchanged site.

Autoreductions	ΔE_{auto} (kcal/mol)
one-ion exchanged Cu^{2+} ZSM-5(T6T12) → one-ion exchanged Cu^+ ZSM-5 (T6T12, Cu^+ at T6) → one-ion exchanged Cu^+ ZSM-5 (T6T12, Cu^+ at T12)	217.76 220.08
one-ion exchanged Cu^{2+} ZSM-5(T8T8) → one-ion exchanged Cu^+ ZSM-5 (T8T8, Cu^+ at T8) → one-ion exchanged Cu^+ ZSM-5 (T8T8, Cu^+ at T'8)	188.09 195.89
one-ion exchanged Cu^{2+} ZSM-5(T7T12-model1) → one-ion exchanged Cu^+ ZSM-5 (T7T12-model1, Cu^+ at T7) → one-ion exchanged Cu^+ ZSM-5 (T7T12-model1, Cu^+ at T12)	188.03 148.93
one-ion exchanged Cu^{2+} ZSM-5(T7T12-model2) → one-ion exchanged Cu^+ ZSM-5 (T7T12-model2, Cu^+ at T7) → one-ion exchanged Cu^+ ZSM-5 (T7T12-model2, Cu^+ at T12)	208.03 203.84

สถาบันวิทยบริการ
จุฬาลงกรณ์มหาวิทยาลัย

5.6 Combined Exchanged and Autoreduction Energy of Cu^{2+} at T6T12, T8T8, T7T12-model1, and T7T12-model2 Exchanged Site

Combined ΔE_{exch} and ΔE_{auto} of Cu^{2+} resided at various exchanged sites were given in Table 5.17. The combined energies of Cu^{2+} in ZSM-5 are smaller than ΔE_{auto} of Cu^{2+} in aqueous solution (256.04 kcal/mol), except T7T12-model1, Cu at T12.

Table 5.17 Combined ΔE_{exch} and ΔE_{auto} of Cu^{2+} in ZSM-5 at T6T12, T8T8, T7T12-model1, and T7T12-model2 exchanged site.

Exchanges + Autoreductions	$\Delta E_{\text{exch}} + \Delta E_{\text{auto}}$ (kcal/mol)
one-ion exchanged Cu^{2+} ZSM-5(T6T12)	
→ one-ion exchanged Cu^+ ZSM-5 (T6T12, Cu^+ at T6)	226.95
→ one-ion exchanged Cu^+ ZSM-5 (T6T12, Cu^+ at T12)	229.77
one-ion exchanged Cu^{2+} ZSM-5(T8T8)	
→ one-ion exchanged Cu^+ ZSM-5 (T8T8, Cu^+ at T8)	236.95
→ one-ion exchanged Cu^+ ZSM-5 (T8T8, Cu^+ at T'8)	244.75
one-ion exchanged Cu^{2+} ZSM-5(T7T12-model1)	
→ one-ion exchanged Cu^+ ZSM-5 (T7T12-model1, Cu^+ at T7)	256.78
→ one-ion exchanged Cu^+ ZSM-5 (T7T12-model1, Cu^+ at T12)	217.68
one-ion exchanged Cu^{2+} ZSM-5(T7T12-model2)	
→ one-ion exchanged Cu^+ ZSM-5 (T7T12-model2, Cu^+ at T7)	251.80
→ one-ion exchanged Cu^+ ZSM-5 (T7T12-model2, Cu^+ at T12)	247.61

จุฬาลงกรณ์มหาวิทยาลัย

CHAPTER 6

DISCUSSIONS

6.1 Optimized Structures of HZSM-5

According to Figs. 5.1-5.4, the optimized HZSM-5 structures are indicated. For all HZSM-5 cluster models, T6T12, T8T8, T7T12-model1 and T7T12-model2 site show the same O-H bond length of 0.96 Å and show T-O-H bond angles between 115.33° and 118.98°. For O-H⁺ distances, they are 0.99 Å for T6T12 site, 0.98 Å for T8T8 and T7T12-model2 site, and 0.97 and 0.98 Å for T7T12-model1 site. This suggests that H⁺ bound to O⁻ in ≡Al-O⁻-Si≡, except T7T12-model1 where H⁺ bound to O at the terminal TOH. All H⁺ were found in the channel of HZSM-5. Since, O-H⁺ distances are very short around 0.98 Å similar to OH bond of water, therefore H⁺ binds to the acidic oxygen very strongly. Among 6-T-ring cluster T7T12-model1 has the lowest energy and, hence, is the most stable site for 6-T-ring cluster. The 5-T-ring cluster T6T12 could not be directly compared. The energies must be compared to evaluate the stability of H⁺.

6.2 Optimized Structures of One-ion Exchanged Cu²⁺ZSM-5

According to Figs. 5.5-5.8, and Tables 5.1-5.4, the optimized Cu²⁺ZSM-5 structures and their parameters are indicated. The coordination number of Cu²⁺ could be determined from Cu²⁺-O distance. The coordinate of Cu²⁺ is established if the Cu²⁺-O distance is around 2 Å. Thus, Cu²⁺ has coordination numbers of 2 for all exchanged sites; T6T12, T8T8, T7T12-model1, and T7T12-model2. For 6-T-ring, the Cu²⁺ is located near O1 and O3 with the distances of 1.93 and 1.92 Å for T8T8 site, near O1 and O4 with the distances of 1.96 and 1.95 Å for T7T12-model1, and near O3 and O6 with the distance of 1.95 and 2.02 Å for T7T12-model2. For 5-T-ring, T6T12, Cu²⁺ is located near O1 and O3 with the distances of 1.96 and 1.99 Å.

6.3 Optimized Structures of One-ion Exchanged Cu⁺ZSM-5

According to Figs. 5.9-5.16, and Tables 5.6-5.9, the O-H⁺ distances for all sites are found to be between 0.97 and 1.00 Å. From Table 5.6, Cu⁺-O distances of 1.89-5.33 Å were found for T6T12 site where Cu⁺ at T6, and of 1.93-3.91 Å for T6T12 site where Cu⁺ at T12. For T6T12, Cu⁺ at T6, Cu⁺ is located near O'1 with the distance of 1.89 Å, and for T6T12, Cu⁺ at T12, Cu⁺ is located near O3 and O4 with the distances of 2.03 and 1.93 Å respectively,. From Table 5.7, Cu⁺-O distances of 1.96-3.77 Å for one-ion exchanged Cu⁺ZSM-5(T8T8, Cu⁺ at T8), and of 1.75-3.85 Å for one-ion exchanged Cu⁺ZSM-5(T8T8, Cu⁺ at T8'). When Cu⁺ at T8, it is located near O1 and O6 with the distances of 2.02 and 1.96 Å, respectively. When Cu⁺ at T8', it is near O3 and O4 with the distances of 1.92 and 1.75 Å, respectively. For Table 5.8, Cu⁺-O distances of 1.89-4.53 Å for Cu⁺ZSM-5(T7T12-model1, Cu⁺ at T7), and of 1.98-3.51 Å for Cu⁺ZSM-5(T7T12-model1, Cu⁺ at T12). When Cu⁺ at T7, it is located near O1 and O'1 with the distances of 1.98 and 1.89 Å, respectively. And when Cu⁺ at T12, it is located near O4 with the distances of 1.98 Å. For Table 5.9, Cu⁺-O distances of 1.93-4.19 Å for Cu⁺ZSM-5(T7T12-model2, Cu⁺ at T7), and of 1.99-3.98 Å for Cu⁺ZSM-5(T7T12-model2, Cu⁺ at T12). When Cu⁺ at T7, it is located in the ring plane near O6 with the distance of 1.93 Å, respectively. And when Cu⁺ at T12, it is located near O3 with the distances of 1.99 Å. The O-H⁺ distances are longer than in HZSM-5 while Cu⁺-O distance is similar to two-ion exchanged Cu⁺ZSM-5.

6.4 Optimized Structures of Two-ion Exchanged Cu⁺ZSM-5

According to Figs. 5.17-5.20, and Tables 5.11-5.14, distances between Cu⁺ are in the range of 2.23-2.39 Å. These values are the longest for T6T12 site and shortest for T7T12-model2 site. Distances between Cu⁺ and skeleton O are between 1.88-4.85 Å. For T6T12, Cu⁺-O distances are in the range of 1.96-4.85 Å, which one Cu⁺ is near O1 and O3 with the distances of 2.00 Å and another Cu⁺ is near O5 with the distance of 1.96 Å. For T8T8, Cu⁺-O distances are in the range of 1.94-3.90 Å, which one Cu⁺ is near O3 and O4 with the distances of 2.02 Å and another Cu⁺ is near O6 with the distance of 1.94 Å. For T7T12-model1, Cu⁺-O distances are found to be between 1.88-4.28 Å, which One Cu⁺ is located near O1 and O4 with the distances of 1.98 and

1.99 Å, respectively, and another Cu⁺ is located near O'1 with distance of 1.88 Å. For T7T12-model2, Cu⁺-O distances are in the range of 2.01-3.99 Å, which One Cu⁺ is located near O3 with the distances of 2.01Å, and another Cu⁺ is located near O5 and O6 with distance of 2.02 Å. Since, Cu⁺ is near to each other, thus, the complex with 2 Cu⁺ is rather unstable.

6.5 Exchanged Energy of Cu Species in ZSM-5 at T6T12, T8T8, T7T12-model1, and T7T12-model2 Exchanged Site at Room Temperature

Exchanged energy (ΔE_{exch}) of one- and two-ion exchanged CuZSM-5 were calculated and shown in Table 5.5, 5.10, and 5.15. For bare Cu ion species, these ΔE_{exch} are positive which means that Cu should not exchanged to ZSM-5 as bare Cu ion. For one-ion exchanged Cu²⁺ZSM-5, exchange at T6T12 has the lowest energy (9.19 kcal/mol) while at T7T12-model1 has the highest (68.75 kcal/mol). Although it has positive ΔE_{exch} , exchange of Cu²⁺ at T6T12 site is still possible. For two-ion exchanged Cu⁺ZSM-5, all exchanged sites have the ΔE_{exch} exceeding 100 kcal/mol, T6T12 has the lowest ΔE_{exch} 143.29 kcal/mol. This suggests that the two-ion exchanged Cu⁺ZSM-5, exchange is rather impracticable. The large ΔE_{exch} is probably due to electrostatic repulsion between two bare Cu⁺ ions. For single H⁺ exchanged Cu⁺ZSM-5, ΔE_{exch} with the range of 66.62-105.72 kcal/mol was obtained. The site with the lowest ΔE_{exch} is T7T12-model1. Since the ΔE_{exch} is very high, the exchange of Cu⁺ is rather unstable and should not take place. The large ΔE_{exch} again comes from the repulsion between Cu⁺ and H⁺, this repulsion is less than between two Cu⁺ ions.

6.6 Autoreduction of Cu²⁺ to Cu⁺ in ZSM-5 at T6T12, T8T8, T7T12-model1, and T7T12-model2 Exchanged Site at Room Temperature

Consider the autoreduction of Cu²⁺ to Cu⁺ in aqueous solution and in the cavity of ZSM-5 at various exchanged sites. In aqueous solution, taken account solvent effects, we found the autoreduction energy (ΔE_{auto}) of 256.04 kcal/mol. To compare ΔE_{auto} in aqueous solution and ΔE_{auto} in the exchanged sites that were listed in Table 5.16, it was found that ΔE_{auto} for all exchanged sites; T6T12, T8T8, T7T12-model1, and T7T12-model2, are lower than 256.04 kcal/mol. And T7T12-model1 is

the lowest ΔE_{auto} of 148.93 kcal/mol. This suggests that the autoreductions of Cu^{2+} to Cu^+ for all exchanged sites can be taken place easier than in aqueous solution.

When consider combined ΔE_{exch} and ΔE_{auto} (Table 5.17), most of the combined energies is smaller than 256.04 kcal/mol. This was confirmed that conversion Cu^{2+} to Cu^+ in the cavity of ZSM-5 are easier than in aqueous solution. Still, the conversion at these sites is very low at room temperature.



สถาบันวิทยบริการ
จุฬาลงกรณ์มหาวิทยาลัย

CHAPTER 7

CONCLUSIONS

7.1 Optimized Structures of HZSM-5 and CuZSM-5 Exchanged Sites

When all exchanged sites are considered, H^+ , Cu^{2+} , and Cu^+ are located in the cavity of ZSM-5. The distances are varied between 0.97-1.00 Å for $O-H^+$, 1.92-4.17 Å for $Cu^{2+}-O$, and 1.75-5.33 Å for Cu^+-O . For all exchanged sites; T6T12, T8T8, T7T12-model1, and T7T12-model2, Cu species form either mono- or bi- coordination.

7.2 Exchanged Energy of Cu Species in ZSM-5 at Room Temperature

The exchanged energies (ΔE_{exch}) at all exchanged sites show positive values. Thus, it is very unlikely for Cu to be exchanged as bare Cu ion except for Cu^{2+} at T6T12 site, Exchange of Cu^+ for two-ion exchanged Cu^+ZSM-5 has the largest energy followed by one-ion exchanged Cu^+ZSM-5 and one-ion exchanged $Cu^{2+}ZSM-5$ has the lowest ΔE_{exch} . The instability of two- and one-ion exchanged Cu^+ZSM-5 is due to the repulsion between charged species, Cu^+-Cu^+ and Cu^+-H^+ , respectively. The most stable exchanged species is Cu^{2+} and the most favorable exchanged site is T6T12 with ΔE_{exch} of 9.19 kcal/mol.

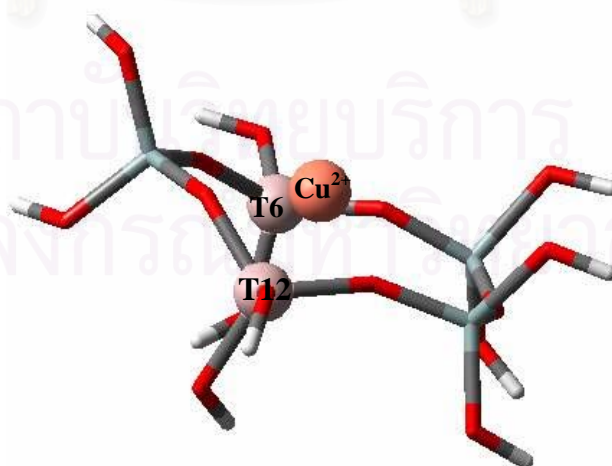


Fig. 7.1 The most favorable exchange site; one-ion exchanged $Cu^{2+}ZSM-5(T6T12)$.

7.3 Autoreduction of Cu^{2+} to Cu^+ in ZSM-5 at T6T12, T8T8, T7T12-model1, and T7T12-model2 Exchanged Site at Room Temperature

Autoreduction energy (ΔE_{auto}) of Cu^{2+} show high positive value for both in aqueous solution (256.04 kcal/mol) and in the cavity of ZSM-5. Thus, the autoreduction of bare Cu^{2+} to Cu^+ should not take place. However, the ΔE_{auto} for all exchanged sites; T6T12, T8T8, T7T12-model1, and T7T12-model2, are lower than 256.04 kcal/mol. This suggests that the autoreduction of Cu^{2+} in ZSM-5 is more competitive than in aqueous solution. When consider combined energy between ΔE_{exch} and ΔE_{auto} , most of the combined energy is still smaller than 256.04 kcal/mol. The exchange of Cu^{2+} and conversion to Cu^+ in ZSM-5 is competitive than in aqueous. However, the autoreduction of Cu^{2+} in ZSM-5 at room temperature, if exists, should take other routes.

Suggestions for Future Work

For the characterization of copper active sites in the cavity of ZSM-5, exchange of other copper species such as $[\text{Cu}(\text{H}_2\text{O})_n]^{2+}$, $[\text{Cu-O-Cu}]^{2+}$, etc., should be investigated. Furthermore, the mechanism of NO_x decomposition by the Cu species should be also investigated.

REFERENCES

1. Breck, D. W. Zeolite Molecular Sieves: Structure, Chemistry, and Use. Florida: Robert E. Krieger Publishing Company, **1973**.
2. Meimer, W. M.; Olson, D. H. Atlas of Structure Type. London: Butterworth-Heinemann, **1992**.
3. Dyer, A. An Introduction to Zeolite Molecular Sieves. New York: John Wiley & Sons., **1988**.
4. Olson, D. H.; Kokotailo, G. T.; Lawton, S. L.; Meier, W. M. "Crystal Structure and Structure-Related Properties of ZSM-5", *J. Phys. Chem.*, **1981**, 85, 2238-2243.
5. Sayle, D. C.; Catlow, C. R. A.; Gale, J. D.; Perrin, M. A.; Nortier, P. "Computer Modeling of the Active-Site Configurations within the NO Decomposition Catalyst Cu-ZSM-5", *J. Phys. Chem. A.*, **1997**, 101, 3331-3337.
6. Yongsheng, L; Jinqu, W; Jianlin, S; Xiongf, Z; Jinming, L; Zhongying, B; Dongsheng, Y. "Synthesis of ZSM-5 zeolite membranes with large area on porous, tubular α -Al₂O₃ supports", *Sep. Purif. Technol.*, **2003**, 32, 397-401.
7. Atsushi, I; Yasushige, K; Mahiko, N. "Elucidation of a preparation method for copper on-exchanged ZSM-5 Samples exhibiting extremely efficient N₂-adsorption at room temperature: effect of counter ions in the exchange solution", *Micropor. Mesopor. Mater.*, **2004**, 70, 119-126.
8. Trout, B. L.; Chakraborty, A. K.; Bell, A. T. "Local Spin Density Functional Theory Study of Copper Ion-exchanged ZSM-5", *J. Phys. Chem.*, **1996**, 100, 4173-4179.
9. Hu, S.; Reimer, J. A.; Bell, A. T. "⁶⁵Cu NMR Spectroscopy of Cu-exchanged ZSM-5 Catalysts", *J. Phys. Chem. B*, **1997**, 101, 1869-1871.
10. Larsen, S.C.; Aylor, A.; Bell, A. T.; Reimer, J. A. "Electron Paramagnetic Resonance Studies of Copper Ion-Exchanged ZSM-5", *J. Phys. Chem.*, **1994**, 98, 11533-11540
11. Teraishi, K.; Ishida, M.; Irisawa, J.; Kume, M.; Takahashi, Y.; Nakano, T.; Nakamura, H.; Miyamoto, A. "Active Site Structure of Cu/ZSM-5: Computational Study", *J. Phys. Chem. B*, **1997**, 101, 8079-8085.

12. Tonkyn, R. G; Barlow, S. E; Hoard, J. W. “Reduction of NO_x in synthetic diesel exhaust via two-step plasma-catalyst treatment”, *Appl. Catal. B: Environ.*, **2003**, 40, 207-217.
13. Shelef, M. “Selective Catalytic Reduction of NO_x with N-free Reductants”, *Chem. Rev.*, **1995**, 95, 209-225.
14. Roberge, D; Raf, A; Kaliaguine, S; Trong On, D; Iwamoto, S. “Selective Catalytic reduction of NO under ambient conditions using ammonia as reducing agent and MFI zeolites as catalyst”, *Appl. Catal. B: Environ.*, **1996**, 10, L237-L243.
15. Iwamoto, M.; Yahiro, H.; Tanada, K.; Mozino, Y.; Mine, Y.; Kagawa, S. “Removal of Nitrogen Monoxide through a Novel Catalytic Process. 1. Decomposition on Excessively Copper Ion Exchanged ZSM-5 Zeolites”, *J. Phys. Chem.*, **1991**, 95, 3727-3730.
16. Iwamoto, M.; Yahiro, H.; Mizuno, N.; Zhang, W.; Mine, Y.; Furukawa, H.; Kagawa, S. “Removal of Nitrogen Monoxide through a Novel Catalytic Process. 2. Infrared Study on Surface Reaction of Nitrogen Monoxide Adsorbed on Copper Ion-Exchanged ZSM-5 Zeolites”, *J. Phys. Chem.*, **1992**, 96, 9360-9366.
17. Iwamoto, M.; Furukawa, H.; Kagawa, S. In New Developments in Zeolite Science and Technology. Amsterdam: Elsevier, **1986**.
18. Warren, J. H; Leo, R; Paul, v.R. S; John, A.P. Ab initio molecular orbital theory. New York: John Wiley & Sons., **1985**.
19. Mark, A. R; Geoge, C. S. Introduction to quantum mechanics in chemistry. Prentice: New Jersey, **2000**.
20. Szabo, A., Ostlund, N. S. “Modern Quantum Chemistry: Introduction to Advanced Electronic Structure Theory”, New York: MacMillan Publishing Co., **1982**.
21. Slater, J. C. “A Simplification of the Hartree-Fock Method”, *Phys. Rev.*, **1951**, 81, 385-390.
22. Hehre, W. J., Ditchfield, R., Pople, J. A. “Self-Consistent Molecular Orbital Methods. XII. Further Extensions of Gaussian-Type Basis Sets for Use in Molecular Orbital Studies of Organic Molecules”, *J. Chem. Phys.*, **1972**, 56, 2257-2261.

23. Kohn, W.; Becke, A. D.; Parr, R. G. "Density Functional Theory of Electronic Structure", *J. Phys. Chem.*, **1996**, 100, 12974-12980.
24. Dirac, P. A. M. "Note on Exchange Phenomena in the Thomas Atom", *Proc. Camb. Phil. Soc.*, 1930, 26, 376-385.
25. Hohenberg, P; Kohn, W. "Inhomogeneous Electron Gas", *Phys. Rev.*, **1964**, 136, B864-B871.
26. Kohn, W.; Sham, L. J. "Self Consistent Equations Including Exchange and Correlation Effects", *Phys. Rev.*, **1965**, 140,A1133-A1138.
27. Vosko, S. J., Wilk, L., Nusair, M. "Accurate Spin-Dependent Electron Liquid Correlation Energies for Local Spin Density Calculations: A Critical Analysis", *Can. J. Phys.*, **1980**, 58, 1200-1211.
28. Becke, A. D. "Density Functional Calculations of Molecular Bond Energies", *J. Chem. Phys.*, **1986**, 84, 4524-4529.
29. Perdew, J. P., Wang, Y. "Accurate and Simple Density Functional for the Electronic Exchange Energy: Generalized Gradient Approximation", *Phys. Rev. B*, 1986, 33, 8800-8802.
30. Becke, A. D. "A Multicenter Numerical Integration Scheme for Polyatomic Molecules", *J. Chem. Phys.*, **1988**, 88, 2547-2553.
31. Lee, C., Yang, W., Parr, R. G. "Development of the Colle-Salvetti Correlation-Energy Formula into a Functional of the Electron Density", *Phys. Rev. B*, **1988**, 37, 785-789.
32. Perdew, J. P., Wang, Y. "Accurate and Simple Analytic Representation of the Electron Gas Correlation Energy", *Phys. Rev. B.*, 1992, 45, 13244-13249.
33. Perdew, J. P., Burke, K., Ernzerhof, M. "Generalized Gradient Approximation Made Simple", *Phys. Rev. Lett.*, **1996**, 77, 3865-3868.
34. Frisch, M. J.; Trucks, G. W.; H. B. Schlegel, G. E. S.; Robb, M. A.; Cheeseman, J. R.; Zakrzewski, V. G.; Montgomery, J. A.; Stratmann, R. E.; Burant, J. C.; Dapprich, S.; Millam, J. M.; Daniels, A. D.; Kudin, K. N.; Strain, M. C.; Farkas, O.; Tomasi, J.; Barone, V.; Cossi, M.; Cammi, R.; Mennucci, B.; Pomelli, C.; Adamo, C.; Clifford, S.; Ochterski, J.; Petersson, G. A.; Ayala, P. Y.; Cui, Q.; Morokuma, K.; Malick, D. K.; Rabuck, A. D.; Raghavachari, K.; Foresman, J. B.; Cioslowski, J.; Ortiz, J. V.; Stefanov, B. B.; Liu, G.; Liashenko, A.; Piskorz, P.;

Komaromi, I.; Gomperts, R.; Martin, R. L.; Fox, D. J.; Keith, T.; Al-Laham, M. A.; Peng, C. Y.; Nanayakkara, A.; Gonzalez, C.; Challacombe, M.; Gill, P. M. W.; Johnson, B. G.; Chen, W.; Wong, M. W.; Andres, J. L.; Head-Gordon, M.; Replogle, E. S.; Pople, J. A. Gaussian 98 (ReVision A.7) (Theory and Calculation). Pittsburgh: PA, **1998**.

35. Poompub, U. Structures and Acidities of H-ZSM-5 with Si/Al Ratio of 47 and 95. (Master's Thesis, Petrochemistry and Polymer Science, Faculty of Science, Graduate School, Chulalongkorn University, Thailand, **2004**).



สถาบันวิทยบริการ
จุฬาลงกรณ์มหาวิทยาลัย

CURRICULUM VITAE

Pengunya Unjit

1979 Born September 7th, in Trang, Thailand

Father : Mr. Pol Unjit

Mother : Mrs. La-ong Unjit

1984-1990 Elementary School (Banklongpasi School, Trang)

1990-1993 Primary School (Kantangpithayakorn School, Trang)

1993-1996 High School (Suan-anan School, Bangkok)

1996-2000 Bachelor of Science (Chemistry),
Prince of Songkhla University, Songkhla

2000-2004 Master degree student at department of Chemistry,
Chulalongkorn University, Bangkok

สถาบันวิทยบริการ
จุฬาลงกรณ์มหาวิทยาลัย